



Universidade Federal
do Rio de Janeiro

Escola Politécnica

On Equalization Performance in Underwater Acoustic Communication System

Vinicius Mesquita de Pinho

Projeto de Graduação apresentado ao Curso de Engenharia Eletrônica e de Computação da Escola Politécnica, Universidade Federal do Rio de Janeiro, como parte dos requisitos necessários à obtenção do título de Engenheiro.

Orientadores: Marcello L. R. de Campos e
Rafael da Silva Chaves

Rio de Janeiro
Fevereiro de 2019

On Equalization Performance in Underwater Acoustic
Communication System

Vinicius Mesquita de Pinho

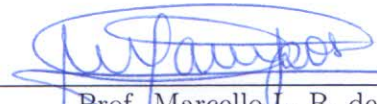
PROJETO DE GRADUAÇÃO SUBMETIDO AO CORPO DOCENTE DO CURSO
DE ENGENHARIA ELETRÔNICA E DE COMPUTAÇÃO DA ESCOLA POLITÉCNICA
DA UNIVERSIDADE FEDERAL DO RIO DE JANEIRO COMO PARTE DOS
REQUISITOS NECESSÁRIOS PARA A OBTENÇÃO DO GRAU DE ENGEN-
HEIRO ELETRÔNICO E DE COMPUTAÇÃO

Autor:



Vinicius Mesquita de Pinho

Orientador:




Prof. Marcello L. R. de Campos, Ph.D.

Orientador:




Rafael da Silva Chaves, M.Sc.

Examinador:



Prof. Sergio Lima Netto, Ph.D.

Examinador:



Prof. Tadeu Nagashima Ferreira, D.Sc.

Rio de Janeiro
Fevereiro de 2019

Declaração de Autoria e de Direitos

Eu, *Vinicius Mesquita de Pinho* CPF 130.274.137-32, autor da monografia *On Equalization Performance in Underwater Acoustic Communication System*, subscrevo para os devidos fins, as seguintes informações:

1. O autor declara que o trabalho apresentado na disciplina de Projeto de Graduação da Escola Politécnica da UFRJ é de sua autoria, sendo original em forma e conteúdo.
2. Excetua-se do item 1. eventuais transcrições de texto, figuras, tabelas, conceitos e ideias, que identifiquem claramente a fonte original, explicitando as autorizações obtidas dos respectivos proprietários, quando necessárias.
3. O autor permite que a UFRJ, por um prazo indeterminado, efetue em qualquer mídia de divulgação, a publicação do trabalho acadêmico em sua totalidade, ou em parte. Essa autorização não envolve ônus de qualquer natureza à UFRJ, ou aos seus representantes.
4. O autor pode, excepcionalmente, encaminhar à Comissão de Projeto de Graduação, a não divulgação do material, por um prazo máximo de 01 (um) ano, improrrogável, a contar da data de defesa, desde que o pedido seja justificado, e solicitado antecipadamente, por escrito, à Congregação da Escola Politécnica.
5. O autor declara, ainda, ter a capacidade jurídica para a prática do presente ato, assim como ter conhecimento do teor da presente Declaração, estando ciente das sanções e punições legais, no que tange a cópia parcial, ou total, de obra intelectual, o que se configura como violação do direito autoral previsto no Código Penal Brasileiro no art.184 e art.299, bem como na Lei 9.610.
6. O autor é o único responsável pelo conteúdo apresentado nos trabalhos acadêmicos publicados, não cabendo à UFRJ, aos seus representantes, ou ao(s) orientador(es), qualquer responsabilização/ indenização nesse sentido.
7. Por ser verdade, firmo a presente declaração.



Vinicius Mesquita de Pinho

UNIVERSIDADE FEDERAL DO RIO DE JANEIRO

Escola Politécnica - Departamento de Eletrônica e de Computação

Centro de Tecnologia, bloco H, sala H-217, Cidade Universitária

Rio de Janeiro - RJ CEP 21949-900

Este exemplar é de propriedade da Universidade Federal do Rio de Janeiro, que poderá incluí-lo em base de dados, armazenar em computador, microfilmear ou adotar qualquer forma de arquivamento.

É permitida a menção, reprodução parcial ou integral e a transmissão entre bibliotecas deste trabalho, sem modificação de seu texto, em qualquer meio que esteja ou venha a ser fixado, para pesquisa acadêmica, comentários e citações, desde que sem finalidade comercial e que seja feita a referência bibliográfica completa.

Os conceitos expressos neste trabalho são de responsabilidade do(s) autor(es).

A Kátia, Valdecy e Amanda os dias todos.

AGRADECIMENTOS

Sinto que este agradecimento será extenso, pois sou muito privilegiado e tenho muito a agradecer.

Primeiro, devo agradecer às pessoas que são responsáveis por tudo em minha vida. Meus pais, Valdecy e Kátia e minha irmã, Amanda. Vocês são a base de tudo o que fui, sou e serei. A vocês todo amor do mundo. Serei sempre grato a vocês em todos os momentos de minha vida.

De forma muito especial, gostaria de agradecer ao meu orientador, Marcello. O que você fez por mim durante a caminhada que me trouxe até aqui é motivo para eu ser grato pelo resto de minha vida. Obrigado por sempre acreditar em mim, e pela oportunidade de ser seu aluno. Minha eterna gratidão.

Agora, a pessoa que talvez mais tenha sofrido com esse projeto, meu orientador Rafael. Obrigado por nunca desistir de mim e pela paciência com as eventuais lerdezas minhas (risos). Tenho certeza que você está no caminho certo na vida, terei orgulho de dizer que fui seu primeiro orientado em um projeto de graduação. Muito obrigado, meu amigo.

Se o SMT-2 virou quase uma segunda casa, as pessoas que estiveram comigo nesta jornada têm fundamental importância no meu êxito. Pelos mil intervalos no trabalho para sentar a mesa do café e conversar, pelas eventuais ajudas no texto ou num código, ou simplesmente reclamar das cadeiras do laboratório, que já passaram da hora de serem trocadas. Todos os momentos foram importantes. Obrigado Felipe, Wesley, Cinelli, Igor, Matheus, Roberto, Gabriel, Spelta, Curi e Padilla. Um agradecimento especial a Edinalva, por aturar nossas bagunças no laboratório sempre com paciência e bom humor.

A todos os amigos que me ajudaram e estiveram comigo durante a graduação, vocês foram extremamente importantes para a minha formação tanto pessoal quanto acadêmica. Em especial, duas mulheres incríveis, que são muito importantes para

mim. Rebeca e Renata, tenho certeza de que sem vocês eu nunca terminaria a graduação. Vocês são exemplos que eu seguirei para a vida. O mundo é de vocês. Obrigado.

Não poderia deixar de citar alguns nomes também importantes da graduação que eu gostaria de agradecer, Nicholas, Krishynan, Bruno, Lucas. A todos os outros que sabem que são importantes.

Agora os amigos desta vida que ainda não agradei. Seja no Espírito Santo ou no Rio de Janeiro, vocês sempre tornaram a vida mais leve e agradável, obrigado pela companhia. Este muito obrigado é destinado a todos vocês. Em especial, Ingrid, Domenica, Thalyson, Yuri, Pedro e Fernanda.

Um obrigado especial aos amigos que tiveram a missão, talvez por vezes enfadonha, de dividir apartamento comigo, Heitor e Carol. Vocês são muito importantes em minha vida, obrigado pela paciência e pela sempre boa companhia. Também agradeço a galera do Solar, sou muito grato pela amizade de vocês.

Agradeço aos professores Tadeu e Sergio, que compõem a banca examinadora, por aceitarem o convite para avaliar este trabalho.

RESUMO

O presente trabalho versa sobre a utilização de equalizadores em sistemas de comunicação acústicos subaquáticos, em especial o uso do equalizador turbo em canais submarinos de águas rasas. O trabalho teve por objetivo comparar a performance do equalizador turbo com a performance de equalizadores como o equalizador *zero-forcing*, equalizador *minimum mean square error* e o *decision feedback equalizer*. A comunicação acústica submarina apresenta grandes desafios para a transmissão de dados, sendo a severa interferência intersimbólica a mais expressiva característica apresentada. A interferência intersimbólica ocorre de forma menos intensa nos sistemas de comunicação por radiofrequência no ar, por exemplo. A equalização é uma ferramenta essencial para lidar com a interferência intersimbólica, portanto seu uso em sistemas de comunicação subaquáticos é de extrema importância. A fim de analisar a performance de diferentes equalizadores, um sistema de comunicação simulando um ambiente acústico de águas rasas foi implementado no software MATLAB. A implementação simula desde o transmissor até o receptor de um sistema de comunicação. O canal acústico submarino foi implementado através de uma modelagem que leva em conta diversas características do meio. Portanto, gera-se assim um modelo de canal que reflete de forma competente um canal real. No receptor do sistema, cada equalizador foi testado sob as mesmas condições para que a comparação entre as performances seja justa. A figura de mérito utilizada para comparação da performance entre os equalizadores foi a taxa de erro de *bits*.

Equalização em Sistemas de Comunicação Acústica Subaquáticos

Vinicius Mesquita de Pinho

Fevereiro/2019

Orientador: Marcello L. R. de Campos

Orientador: Rafael da Silva Chaves

Curso: Engenharia Eletrônica e de Computação

Palavras-Chave: equalização, equalizador turbo, acústica submarina, sistemas de comunicação.

ABSTRACT

This work addresses equalization in underwater acoustic communication systems, particularly the use of turbo equalizers in shallow water transmissions. The primary goal is to compare turbo equalizers with other equalizers, namely zero-forcing equalizer, minimum mean square error equalizer, and decision feedback equalizer. The underwater acoustic communication displays broad impairments to data transmission, and the most severe one is intersymbol interference. Equalization is one tool applied to mitigate intersymbol interference; therefore its use in communication systems is vital. Moreover, to analyze the performance of the equalizers, a communication system simulation was built using MATLAB. The simulation uses a reliable underwater acoustic channel simulator, which takes into account environmental characteristics when modeling the channel. The equalizers were examined under the same conditions in order to have reliable results. The figure of merit applied to compare the equalizer performances was the bit-error rate.

On Equalization Performance in Underwater Acoustic Communication System

Vinicius Mesquita de Pinho

February/2019

Advisor: Marcello L. R. de Campos

Advisor: Rafael da Silva Chaves

Course: Eletronics and Computing Engineering

Keywords: equalization, turbo equalizer, underwater acoustic, communication systems.

Contents

List of Figures	xiv
List of Tables	xv
List of Abbreviations	xvi
List of Symbols	xix
1 Introduction	1
1.1 A History of Underwater Acoustic	1
1.2 Applications in Recent Years	3
1.3 Underwater Acoustic Channel Characteristics	4
1.4 Channel Equalization	6
1.5 Text Description	7
1.6 Notation	7
2 Underwater Acoustic Channel Characteristics	9
2.1 Sound Velocity	9
2.2 Propagation Loss	12
2.2.1 Frequency-dependent Absorption	12
2.2.2 Geometric Spreading Loss	13
2.2.3 Scattering Loss	14
2.2.4 Propagation Loss Parametrization	15
2.2.5 Time-Varying Multipath	16
2.3 Ambient Noise and External Interference	17

3	Communication System Model	20
3.1	Transceiver Structure Overview	20
3.2	Transceiver Description	21
3.2.1	Information Source	21
3.2.2	Encoder & Decoder	21
3.2.3	Interleaver & Deinterleaver	23
3.2.4	Modulator & Demodulator	24
3.3	Channel	26
3.3.1	UWA Channel Input-Output Relationship	26
3.3.2	Linear Time-varying Channel with Path-specific Doppler Scales	27
3.3.3	Linear Time-varying Channel with One Common Doppler Scale	28
3.3.4	Linear Time-invariant Channel	29
3.3.5	Digital Implementation	29
3.4	Baseband Signal Model	30
3.5	Channel Estimation	33
4	Equalizers	35
4.1	Zero-forcing Equalizer	35
4.2	Minimum Mean Square Error Equalizer	36
4.3	Decision Feedback Equalizer	38
4.3.1	DFE Filter Derivation Based on MMSE	38
4.3.2	Enhancing the DFE Computational Performance	41
4.4	Turbo Equalizer	42
4.4.1	Separate Equalization <i>versus</i> Joint Equalization	42
4.4.2	The Turbo Principle	44
4.4.3	Derivating the Turbo Equalizer Algorithm	45
4.4.4	On the Effect of Multiple Turbo Iterations	49
5	Simulations & Results	51
5.1	Simulation Scenarios	51
5.1.1	On the Relation Between the Channel Characteristics and Channel Examples	52
5.2	Simulation Results	54

5.2.1	Communication System & Turbo Equalizer Parameters Used on Simulations	54
5.2.2	Bit-error Rate Plots for the Simulations	57
6	Conclusions & Future Work	60
6.1	Conclusions	60
6.2	Future Work	61
	Bibliography	62

List of Figures

1.1	UWA communication network.	5
2.1	Salinity and temperature varying with depth.	10
2.2	Sound speed profile	11
2.3	Relationship between sound speed profile and propagation rays	11
2.4	A ray scattering in an irregular reflective surface.	14
2.5	Attenuation formula model in terms of frequency and distance.	15
2.6	Power spectral density of experimental data	19
3.1	Illustration of the transceiver structure.	21
3.2	An 1/3-rate, $K = 3$ linear convolutional encoder.	22
3.3	Example of block interleaver.	24
3.4	Illustration of modulator and demodulator structure.	25
3.5	UWA communication system analog front-end.	26
3.6	Example of sampling of LTI CIR.	30
4.1	Structure for decision feedback equalizer.	38
4.2	Turbo Equalizer structure.	45
4.3	A SISO equalizer based on linear MMSE estimation.	46
4.4	Constellation of received signal, SNR = 10 dB.	49
4.5	Example on the effect of multiple turbo equalization iterations.	50
5.1	Bathymetric profile.	52
5.2	Example of channels for 500 m and 1 km to illustrate the CIR.	53
5.3	Example of channels for 2 km and 5 km.	54
5.4	Example of 10 km channel.	54
5.5	BER <i>versus</i> SNR plot for different values of W	56

5.6	Effect of non-minimum phase channels.	57
5.7	Bit-error ate for different distances.	58

List of Tables

1.1	Comparison of UWA, EM and optical waves in seawater environments.	5
5.1	Channel Characteristics for Simulation.	52
5.2	Parameters used on simulations to generate the BER plot.	56
5.3	SNR gain (dB) when compared to BER of 10^{-2} for the ZFE.	59
5.4	SNR level (dB) necessary to achieve a BER of 10^{-4}	59

List of Abbreviations

ADC *analog-to-digital convert.*

AWGN *additive white Gaussian noise.*

BER *bit-error rate.*

BPSK *binary phase-shift keying.*

CDMA *code division multiple access.*

CIR *channel impulse response.*

DAC *digital-to-analog convert.*

DFE *decision feedback equalizer.*

DSC *deep sound channel.*

EM *electromagnetic.*

FEC *forward error correction.*

FIR *finite impulse response.*

IEAPM *Institute of Sea Studies Admiral Paulo Moreira.*

ISI *intersymbol interference.*

IUD *independent uniformly distributed.*

LLR *log-likelihood ratio.*

LPF *low-pass filter.*

LTI *linear time-invariant.*

MAP *maximum a posteriori.*

ML *maximum likelihood.*

MLSE *maximum likelihood sequence estimator.*

MLSEQ *maximum likelihood sequence equalizer.*

MMSEE *minimum mean square error equalizer.*

MSE *mean square error.*

PDF *probability density function.*

PSD *power spectral density.*

PSU *practical salinity unit.*

RF *radio frequency.*

RV *random variable.*

SER *symbol error rate.*

SISO *soft-input soft-output.*

SNR *signal-to-noise ratio.*

SOFAR *sound fixing and ranging.*

SONAR *sound navigation and ranging.*

TCM *trellis coded modulation.*

TEQ *turbo equalizer.*

UWA *underwater acoustic.*

WWI *World War I.*

WWII *World War II.*

ZFE *zero-forcing equalizer*.

List of Symbols

α_{ac} Absorption coefficient.

α_p Path amplitude or path gain.

β Spreading exponent.

\mathcal{C} Constellation set, or alphabet set.

c Sound speed in water.

D_{spread} Channel delay spread.

ξ Minimum mean square of error.

E Signal energy per symbol.

f_c Carrier frequency.

f_d Doppler frequency shift.

φ_{max} Channel Doppler rate spread.

f_s Sampling frequency.

Φ Toeplitz matrix form of \mathbf{x} .

\mathbf{H} Toeplitz form of the channel impulse response vector.

\mathbf{h} Channel impulse response vector.

h Channel impulse response.

K Convolutional code constraint length.

λ_{ext} Extrinsic Log-likelihood ratio.

λ Log-likelihood ratio.

$p[k]$ Digital pulse waveform.

P_{gsI} Geometric spreading loss.

$p(\mathbf{x}, t)$ Sound pressure at \mathbf{x} in an instant t .

P_{sI} Scattering loss.

P Number of propagation paths.

P_{aI} Absorptive loss.

P_{att} Propagation loss.

ϱ Number of encoder outputs.

S Salinity in parts per thousand.

\mathbf{s}_{ext} Extrinsic soft information.

\mathbf{s} Soft information.

σ_V^2 Noise variance RV V .

σ_X^2 Transmitted signal variance of RV X .

T_{bI} Period of a block length.

τ Delay.

T_{a} Sampling period.

T Temperature in degree Celsius.

μ_X Mean value of RV X .

\mathbf{v} Baseband digital noise vector.

ν Channel memory.

$\tilde{v}(t)$ Passband analog noise.

$\tilde{\mathbf{v}}$ Passband digital noise vector.

\mathbf{w}_b DFE feedback filter.

\mathbf{w}_f DFE forward filter.

\mathbf{W}_{ZF} ZF equalizer matrix.

\mathbf{W}_{MMSE} MMSE equalizer matrix.

\mathbf{W} General equalizer matrix.

$\mathbf{x}[n]$ Baseband digital transmitted vector.

$x[n]$ Baseband digital transmitted signal.

$\tilde{x}(t)$ Passband analog transmitted signal.

$\tilde{\mathbf{x}}[n]$ Passband digital transmitted vector.

$\tilde{x}[n]$ Passband digital transmitted signal.

\mathbf{y} Baseband digital received vector.

$y[n]$ Baseband digital received signal.

$\tilde{y}(t)$ Passband analog received signal.

$\tilde{y}[n]$ Passband digital received signal.

z Depth in meters.

ζ Wave propagation distance.

Chapter 1

Introduction

1.1 A History of Underwater Acoustic

Marine animals have been using *underwater acoustic* (UWA) communication for millions of years. However, for humankind, one of the first documented ideas of using underwater sound comes from Leonardo da Vinci in 1490 [1]:

“If you cause your ship to stop and place the head of a long tube in the water and place the outer extremity to your ear, you will hear ships at a great distance from you.”

Furthermore, the first mathematical theory about the sound propagation is found in *Philosophiae Naturalis Principia Mathematica* [2], written by Sir Isaac Newton in 1687. Although Newton focused on sound propagating in the air, the same basic ideas can be applied to sound propagating in the water. After Newton’s pioneer work, Colladon and Sturm made a significant advance in the development of UWA theory. In 1827, they provided the first quantitative measurement of sound speed in saline water. They measured the elapsed time between a flash of light and the sound of a submerged ship’s bell heard using an underwater listening tube. Calladon and Sturm’s experiment consisted of a bell suspended from a boat that was struck underwater by means of a lever, which at same time caused a candle to ignite some powder and set off a flash of light [3]. An observer in a second boat used a listening tube to measure the time elapsed between the flash of light and the sound of the bell. They measured a sound speed of 1435 m/s, which was about

2% lower than the currently accepted values [3]. In 1877, Lord Rayleigh wrote the Theory of Sound [4], often regarded as marking the beginning of the modern study of acoustics. The Theory of Sound was the first document to formulate the wave equation, a mathematical equation for describing sound waves that is the basis for all work on acoustics.

In the 1900s, the first practical application of underwater sound appeared. The underwater bells equipped on ships were sounded with a fog horn to measure the offshore distance based on the difference of the airborne and waterborne arrivals [5]. The sinking of the Titanic, in April 1912, may have further encouraged scientific discoveries. A month later after the tragic incident, L. R. Richardson filed a patent for an invention that used underwater sound and its echoes to determine distances in underwater, regardless the existence of an appropriate UWA source. Moreover, also motivated by the Titanic disaster, Reginald Fessenden designed an echo-ranging device, which both produced and detected sounds and was called the *Fessenden oscillator*. During the *World War I* (WWI), the Fessenden oscillator was applied to the detection of submarines, but its rather low operating frequency gave it a very broad beam. The broad beam was unsuitable for detecting small targets, such as contact mines suspended on underwater cables [6]. In order to solve the problem of low frequency, in 1917, Paul Langevin used the piezoelectric effect to build a new echo-ranging system [7]. When a changing voltage is applied to a crystal at the desired frequency, they expand and contract, generating a sound wave [8, 9]. In 1918, for the first time, echoes were observed from a submarine at distances as large as 1500 m [10].

Following the WWI, there was a time of increased discovery about UWA. For example, in 1919, the first scientific paper on UWA was published by H. Lichte, a German scientist, describing the refraction of sound waves produced by temperature and salinity gradients in the ocean [11]. Multiple non-military uses of underwater sound can be traced back to this period, such as the echosounders. The echosounders were a echo-ranging device that became commercially available after WWI. They were invaluable for the task of helping ships avoid running aground in shallow water. Perhaps the first practical application of this device was the use of an echosounder

to select the best route for an underwater telegraph cable between Marseilles, France, and Philippeville, Algeria, in 1922 [12]. At the same period, scientists discovered that low-frequency sound could penetrate into the seafloor, being reflected from individual layers in the sediment [3]. This discovery led to the creation of pictures of what was beneath the seafloor, providing clues to the history of the earth and mechanisms for prospecting for oil and gas beneath the seafloor.

During *World War II* (WWII) the research effort on UWA was mainly focused on improving echo-ranging systems [13], which were later called *sound navigation and ranging* (SONAR). The elements that affect the performance of the SONAR systems are described by what is called the SONAR equation [14]. The SONAR equation includes the source level, sound spreading, sound absorption, reflection losses, ambient noise, and receiver characteristics. Some examples of the research done during WWII focused on the development of these systems, such as: high-frequency acoustics, low-frequency and long-range sound propagation, and measurements of background noise levels in the sea. This research was more relevant to SONAR, used to locate submarines and underwater mines [15].

The fast advancement of UWA continued after WWII. The first application of UWA for communication was an underwater telephone, called *Gertrude*. The underwater telephone was developed in the United States and was built for communication with submerged submarines [16]. This device used single-sideband suppressed carrier amplitude modulation in the frequency range of 8 – 11 kHz. The telephone was capable of transmitting UWA signals over several kilometers [17]. Since then, development on UWA communication has been made in various UWA applications.

1.2 Applications in Recent Years

Simultaneously with the technology advances in last decades, an enormous range of underwater communication applications have emerged. One example of application can be found in global warming research. One of the first studies that helped this subject was called *Heard Island Feasibility Study* [18]. This work was a successful very-long-range UWA transmission between the source in the southern Indian

Ocean and 16 receiver sites. This study showed that it is possible to measure the temperature of the ocean over vast distances. That was the first step in a major international experiment to investigate the heating of the world's oceans [3]. This is an essential subject to the study of climate changes on Earth since the oceans play an essential role in atmospheric temperature [18].

Moreover, on UWA communication applications, the development of underwater vehicles of different sizes and functionalities, such as autonomous underwater vehicles and sea gliders, has enabled underwater applications without human interaction [19]. For example, sea gliders, can be set up in oceans to collect data sample of water over a significant time period, and then send the data back to a control station to be analyzed. These underwater vehicles can be employed to study marine animal life, tracking how some species interact with the environment [20]. Another system are the acoustically controlled robots that have been used to replace divers in performing maintenance of submerged platforms [21]. Other examples of applications can be found in a diversity of areas, from scientific biological research to commercial oil exploration, including governmental coast defense, speech transmission between divers, ocean bottom imaging, daily fish migration, whale tracking, and even treasure discovery [3, 10, 22]. As more systems are deployed in underwater applications, the need for communications through longer distances and with higher data throughput keeps growing. Figure 1.1 depicts a UWA communication network that illustrates many applications previously cited.

1.3 Underwater Acoustic Channel Characteristics

As the urge to use underwater communication grows, the technology involved needs to improve. Wireless underwater communication can use three different types of transmission, namely: acoustic, radio frequency, and optical. However, radio frequency waves are of little use because they are severely attenuated, while optical waves suffer from scattering and need high precision in pointing the laser beams [17, 23]. Meanwhile, UWA transmission is capable of reaching higher distances than *electromagnetic* (EM) radio frequency or optical transmissions [23, 24]. This feature makes acoustic communication the dominant technology for wireless underwater

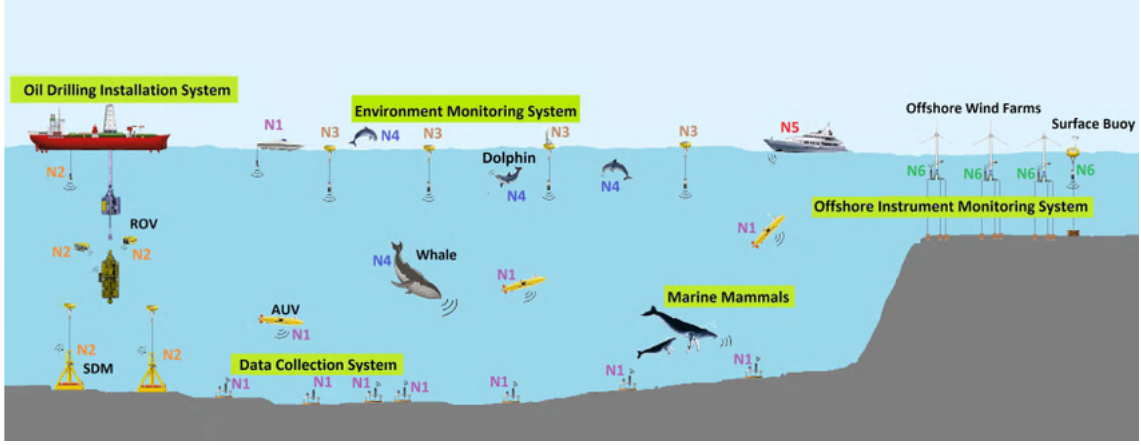


Figure 1.1: UWA communication network, where applications from different areas come together to explore the capabilities of transferring data through the underwater acoustic channel [22].

transmission [23, 25]. Table 1.1 shows a comparison of UWA, EM and optical waves in seawater environments [26].

Table 1.1: Comparison of UWA, EM and optical waves in seawater environments.

	UWA	EM	Optical
Velocity (m/s)	$\sim 1.5 \times 10^3$	$\sim 3 \times 10^8$	$\sim 3 \times 10^8$
Power loss	relatively small	large	\propto turbidity
Bandwidth	\sim kHz	\sim MHz	$\sim 10 - 150$ MHz
Frequency band	\sim kHz	\sim MHz	$\sim 10^{14} - 10^{15}$ Hz
Effective range	\sim km	~ 10 m	$\sim 10 - 100$ m

Besides being a predominant technology, UWA systems have a plethora of problems that hinder its performance and need to be adequately dealt with. These impairments are related to UWA noise [27] and the intense time variations of UWA channels [28, 29]. Moreover, the relative motion between transmitter and receiver, always present in this environment, combined with the low propagation speed of the acoustic waves, aggravates the Doppler effect [24, 30, 31]. Furthermore, the available bandwidth is limited due to the transmission loss, which increases with both frequency and range and restrains high rate transmissions [32, 33].

In general, the UWA channel is modeled as a time-variant linear system due to the Doppler effect [34]. However, in a situation where the Doppler effect can be neglected, the UWA channel becomes a time-invariant system, and the most predominant impairment becomes *intersymbol interference* (ISI) [14]. ISI is mostly induced by the time spread in the received acoustic signal due to the multiple interactions of the signal with sea surface and bottom. As in radio frequency wireless communication in the air, ISI is also harmful in UWA communication and must be appropriately compensated by the transceiver [33]. One of the tools used for mitigating ISI is called channel equalization, which uses some knowledge of the channel state or its impulse response.

1.4 Channel Equalization

The optimum equalizer, from a probability of error viewpoint, is the the *maximum likelihood sequence equalizer* (MLSEQ), which is a type of *maximum a posteriori* (MAP) equalizer [35]. However, the computational complexity of the MLSEQ increases exponentially with channel length. The exponential complexity growth turns the MLSEQ unpractical in UWA communications, because of the long delay spread of the UWA channel [36, 37].

In order to reduce the computational load, suboptimal solutions consisting of linear filters are often employed, such as the *zero-forcing equalizer* (ZFE) [35, 36] and *minimum mean square error equalizer* (MMSEE) [35, 36]. Another solution is the *decision feedback equalizer* (DFE), which exploits the use of previously estimated symbols to reduce ISI [38]. Even though it is not linear, the DFE does not have high complexity and achieves a better performance than ZFE and MMSEE in terms of *bit-error rate* (BER) [39].

Moreover, another alternative is the *turbo equalizer* (TEQ). This equalizer uses an iterative equalization and decoding technique that can achieve impressive performance gains [37, 40]. The TEQ approaches the performance of a MAP receiver by iteratively passing soft information, i.e., statistical information, between the *soft-input soft-output* (SISO) equalizer and the SISO decoder [41, 42]. The idea of

solving the equalization problem iteratively is based on decoding methods for turbo codes [43]. The TEQ repeats the equalization and decoding tasks on the same set of received data, where feedback information from the decoder is incorporated into the equalization process [44]. The TEQ is capable of achieving lower BER than ZFE, MMSEE and DFE within a few iterations.

1.5 Text Description

This first chapter was the Introduction, and the rest of the text is organized as follows: the second chapter introduces us to the underwater acoustic world, where some of the channel characteristics are detailed. Moreover, the third chapter shows how a communication system can overcome the impairments of the underwater acoustic channel, showing all the elements presented in a communication system. Chapter 4 details the part of the communication system that this project focuses on, the equalizers, where four of them are presented. In the sequence, some simulations are described along with its results in order to see the equalizers working and evaluate their performances. Conclusions are draw in Chapter 6 along with some thoughts on future work.

1.6 Notation

Throughout this work, vectors and matrices are represented in bold face with lower case and uppercase letters, respectively. The symbols \mathbb{C} , \mathbb{R} , and \mathbb{N} denote the set of complex, real, and natural numbers, respectively. Consider $M, K \in \mathbb{N}_+$, the symbols $\mathbf{0}_{M \times K}$ and \mathbf{I}_M denote an $M \times K$ matrix with zeros, and an $M \times M$ identity matrix, respectively.

Given the matrix $\mathbf{A} \in \mathbb{C}^{M \times K}$, the notations \mathbf{A}^T , \mathbf{A}^* , \mathbf{A}^H , \mathbf{A}^{-1} , and $\text{Tr}\{\mathbf{A}\}$ stand for transpose, conjugate, Hermitian (conjugate transpose), inverse and trace operations on \mathbf{A} , respectively. Matrix \mathbf{A} can be represented as follows:

$$\begin{aligned}\mathbf{A} &= \begin{bmatrix} a_{11} & a_{12} & \dots & a_{1K} \\ a_{21} & a_{22} & \dots & a_{2K} \\ \vdots & \vdots & \ddots & \vdots \\ a_{M1} & a_{M2} & \dots & a_{MK} \end{bmatrix}, \\ &= \begin{bmatrix} \mathbf{a}_1 & \mathbf{a}_2 & \dots & \mathbf{a}_K \end{bmatrix},\end{aligned}\tag{1.1}$$

where $\mathbf{a}_k \in \mathbb{C}^{M \times 1}$ is the k th column of \mathbf{A} . Moreover, the notation $\mathbf{A} [M_1 : M_2, K_1 : K_2]$ is the representation of the matrix

$$\mathbf{A} [M_1 : M_2, K_1 : K_2] = \begin{bmatrix} a_{M_1 K_1} & \dots & a_{M_1 K_2} \\ \vdots & \ddots & \vdots \\ a_{M_2 K_1} & \dots & a_{M_2 K_2} \end{bmatrix}.\tag{1.2}$$

The notation $\text{Diag}\{\mathbf{x}\}$ stands for the diagonal matrix composed by the elements of \mathbf{x} , i.e.,

$$\begin{aligned}\mathbf{X} &= \text{Diag}\{\mathbf{x}\}, \\ &= \begin{bmatrix} x_1 & & & \\ & x_2 & & \\ & & \ddots & \\ & & & x_M \end{bmatrix}.\end{aligned}\tag{1.3}$$

The scalar $X \in \mathbb{C}$ stands for a random variable, the vector $\mathbf{x} \in \mathbb{C}^{M \times 1}$ stands for a random vector, the scalar $x \in \mathbb{C}$ stands for a realization of X , and the vector $\mathbf{x} \in \mathbb{C}^{M \times 1}$ stands for a realization of \mathbf{x} . The notation $\mathbb{E}\{\mathbf{x}\}$ stands for the expected value of \mathbf{x} . The notation $\mathbf{s}(\cdot)$ stands for the soft information of (\cdot) . The operation $\text{Cov}\{X, Y\}$ represents the covariance, where

$$\text{Cov}\{X, Y\} = \mathbb{E}\{(X - \mathbb{E}\{X\})(Y - \mathbb{E}\{Y\})\},\tag{1.4}$$

and the variance is a special case of the covariance in which the two variables are identical. $\text{Cov}\{X, X\}$ is given by

$$\text{Cov}\{X, X\} = \text{Var}\{X\} = \sigma_X^2.\tag{1.5}$$

Chapter 2

Underwater Acoustic Channel Characteristics

Given the complexity of UWA environment and the low propagation speed of sound in water, the UWA environment is considered as one of the most challenging channels for communication. This chapter presents some characteristics of the UWA channels and makes some connections with *radio frequency* (RF) channel in the air. These associations are made in order to expose some features that make the UWA environment a complex medium to communicate. The first feature explored is the sound velocity in seawater, what differentiates it and what is influenced by it.

2.1 Sound Velocity

The extremely slow propagation speed of sound through seawater, when compared to the EM wave speed through the air, is an essential factor that distinguishes both transmission techniques. This low velocity results in significant transmission latency for a UWA communication system and generates delay spreading of over tens or even hundreds of milliseconds, which translates into frequency-selective signal distortion for the channel [45].

The sound speed depends on water properties, such as temperature, salinity, and pressure. Figure 2.1 shows how salinity, given in *practical salinity unit* (PSU), and temperature, given in degrees Celsius, vary when the depth increases. Both examples

were generated with data from the experimental measurements made in Arraial do Cabo, RJ (22°58'38.2"S, 42°01'10.4"W), provided by the *Institute of Sea Studies Admiral Paulo Moreira* (IEAPM).

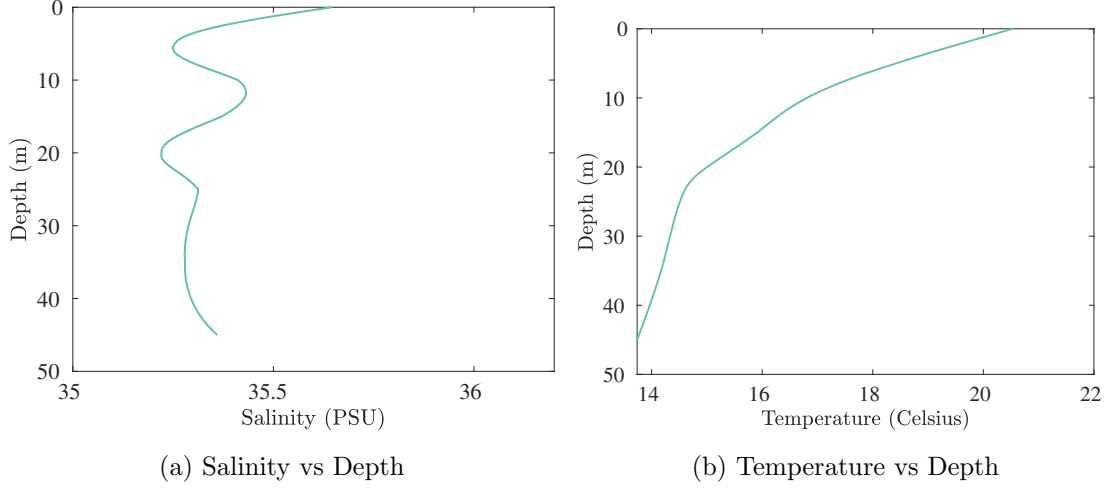


Figure 2.1: Salinity and temperature varying with depth.

A quintessential speed of sound in the water near the ocean surface is about 1500 m/s, which is more than 4 times faster than the speed of sound in air, but 5 orders of magnitude smaller than the speed of light in the air. The speed of sound can be computed using various experimental formulas, which take into account water temperature, salinity, and depth. Some of them are the empirical Mackenzie formula [46], the 19-term equation called NRL II presented in [47], and a simple 6-term equation based on the NRL II proposed in [48]. The sound speed using the Mackenzie formula [46] is written as

$$\begin{aligned}
 c = & 1448.96 + 4.591T - 5.304 \times 10^{-2}T^2 + 2.374 \times 10^{-4}T^3 \\
 & + 1.340(S - 35) + 1.630 \times 10^{-2}z + 1.675 \times 10^{-7}z^2 \\
 & - 1.025 \times 10^{-2}T(S - 35) - 7.139 \times 10^{-13}Tz^3,
 \end{aligned} \tag{2.1}$$

where $T \in \mathbb{R}$ is the temperature in degree Celsius, $S \in \mathbb{R}_+$ is the salinity in parts per thousand, and $z \in \mathbb{R}_+$ is the depth in meters. Demonstrating how velocity of sound behaves in underwater, Figure 2.2 illustrates a sound profile as a function of the depth. The sound speed profile was computed employing the data from Figures 2.1a and 2.1b, and using the Mackenzie formula in (2.1).

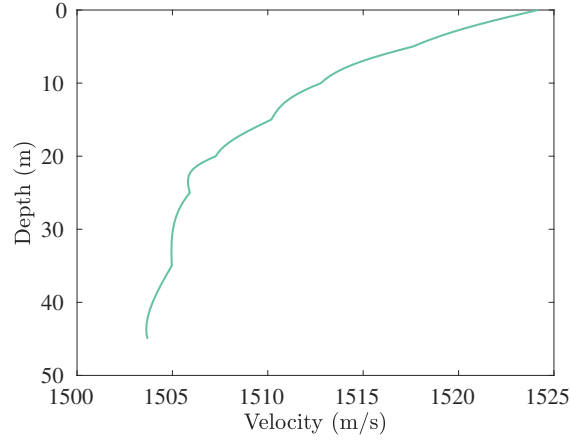


Figure 2.2: Sound speed profile illustrating how velocity changes with increasing the depth in shallow water.

In shallow water, the sound speed is usually considered constant throughout the water column because the velocity variation is small when compared to deep water environments [27], as can be seen in Figure 2.3. This is reflected on how the propagating ray is modeled. For shallow water the propagation is typically represented as illustrated in Figure 2.3a, and for deep water channels it is depicted as in Figure 2.3b. The deep water channel is often called *deep sound channel* (DSC), and the corresponding propagation is called *sound fixing and ranging* (SOFAR) [27].

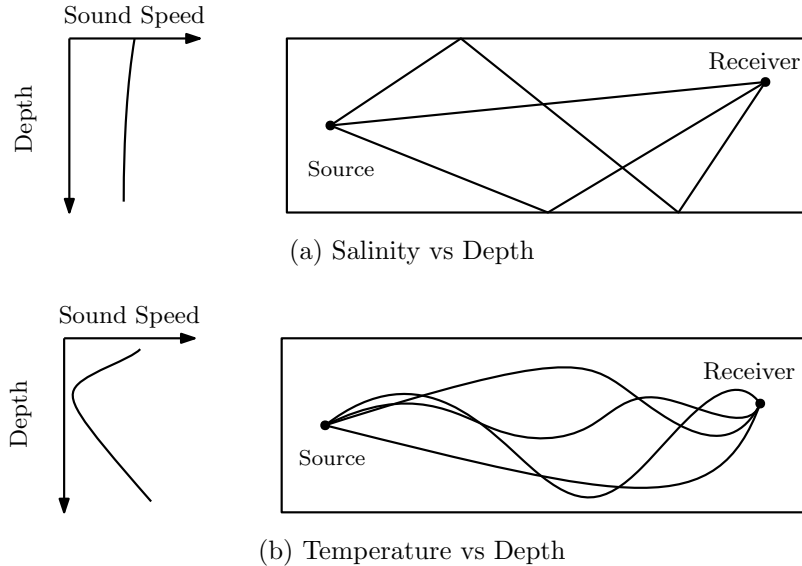


Figure 2.3: How sound velocity variations affect sound propagation rays for both shallow and deep waters transmissions.

In the SOFAR propagation, an interesting situation may happen, a ray that travels a longer distance can get to the receiver before the one that crosses a shorter distance. This phenomenon occurs because the sound speed starts increasing in a certain depth, as can be seen in Figure 2.3b, so the ray covers a greater length in less time than the one which travels in shallower depth [10].

2.2 Propagation Loss

Independently of traveling through shallow or deep water, the acoustic wave is still going to suffer from energy loss, related to the propagation, due to dispersive mechanisms present in the environment. There are three primary causes of energy loss during the propagation of acoustic waves in water: absorptive loss, geometric-spreading loss, and scattering loss [10].

2.2.1 Frequency-dependent Absorption

During the propagation, the wave energy may be transformed into others forms of energy and absorbed by the medium. The medium material imperfection, or the defectiveness in what constitutes the propagation environment, directly affects the absorptive energy loss for the type of physical wave propagating through it. For EM waves, the imperfection is the electric conductivity, whereas for UWA waves, this material imperfection is modeled as the inelasticity, which turns the wave energy into heat. The absorptive loss for UWA wave propagation is frequency-dependent and can be expressed as

$$P_{\text{al}} = e^{\alpha_{\text{ac}}(f)\zeta} \quad (2.2)$$

where $\zeta \in \mathbb{R}_+$ is the propagation distance and $\alpha_{\text{ac}}(f) \in \mathbb{R}$ is the absorption coefficient at frequency $f \in \mathbb{R}_+$ in kHz [10]. For seawater, the absorption coefficient at frequency f can be written as the sum of chemical relaxation processes and absorption from pure water:

$$\alpha_{\text{ac}}(f) = \frac{A_1 P_1 f_1 f^2}{f_1^2 + f^2} + \frac{A_2 P_2 f_2 f^2}{f_2^2 + f^2} + A_3 P_3 f^2 \quad (2.3)$$

where the first term on the right side is the contribution from boric acid, the second term is from the contribution of magnesium sulfate, and the third term is from the

contribution of pure water. $A_1 \in \mathbb{R}$, $A_2 \in \mathbb{R}$ and $A_3 \in \mathbb{R}$ are constants; $P_1 \in \mathbb{R}$, $P_2 \in \mathbb{R}$ and $P_3 \in \mathbb{R}$ model the pressure dependencies; and the relaxation frequencies $f_1 \in \mathbb{R}$ and $f_2 \in \mathbb{R}$ are for the relaxation process in boric acid and magnesium sulfate [28]. In [3], there are formulations of the coefficients A_1 , A_2 , A_3 , P_1 , P_2 , P_3 , f_1 , and f_2 as functions of temperature, salinity, and water depth.

Equation (2.3) can be simplified under mild conditions. For instance, Thorp's formula [49] can be used as absorption model for frequencies less than 50 kHz. In this case, α_{ac} is given by

$$\alpha_{ac}(f) = \frac{0.11f^2}{1+f^2} + \frac{44f^2}{4100+f^2} + 2.75 \times 10^{-4}f^2 + 0.003 \quad (2.4)$$

where $f \in \mathbb{R}_+$ is the frequency in kHz [28].

2.2.2 Geometric Spreading Loss

Geometric-spreading loss is the local power loss of a propagating UWA wave due to energy conservation. When an acoustic impulse propagates away from its source, with increasing distance, the wavefront occupies a surface area that grows. Hence, the wave energy in each unit surface decreases. For the spherical wave generated by a point source, the power loss caused by geometric spreading is proportional to the square of the distance. The spherical wave occurs when acoustic waves spread spherically outward from a source in an unbounded medium [10]. On the other hand, on the cylindrical waves generated by a very long line source, the power loss caused by geometric spreading is proportional to the distance. Moreover, the cylindrical waves occur when acoustic waves spread horizontally because of a medium which has parallel upper and lower bounds.

For a realistic UWA communication setting, the geometric spreading is a combination of spherical and cylindrical spreading, with the power loss being proportional to

$$P_{\text{gs}} = \zeta^\beta, \quad (2.5)$$

where $\zeta \in \mathbb{R}_+$ is the distance traveled by the wave and $\beta \in [1, 2]$, 1 for cylindrical spreading and 2 for spherical spreading [5]. Given that, the sound propagation in

real channels cannot be classified exclusively into either of the two spreading models, a practical value of the spreading exponent can be taken as $\beta = 1.5$ [50].

2.2.3 Scattering Loss

Scattering is the physical process in which irregular surfaces reflect the incident wave in multiple directions, as Figure 2.4 illustrates. The sound scattering in underwater environments can be associated with the nonuniformities in the water column and interactions of UWA waves with nonideal sea surfaces and bottoms. Obstacles in the water column include point targets such as fish and scattering volumes such as fish shoals and bubble clouds. The corresponding scattering loss depends on the acoustic wavelength and target size, and can be modeled by a gain P_{sl} [10, 51].

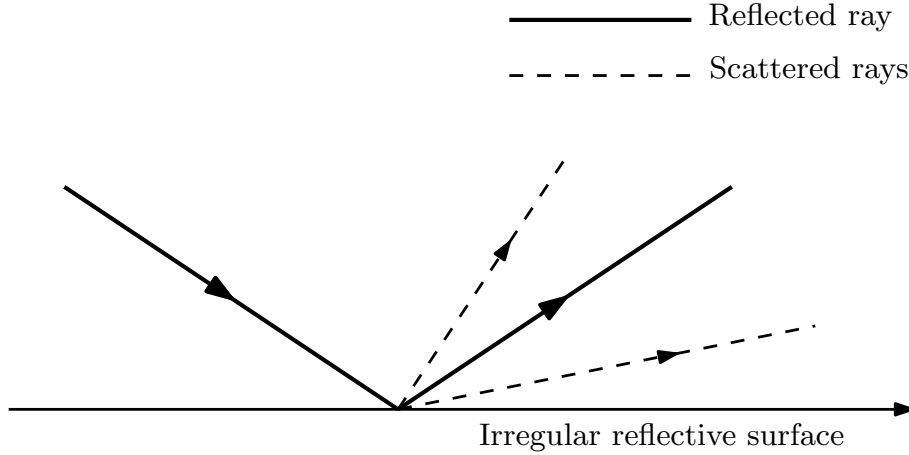


Figure 2.4: A ray scattering in an irregular reflective surface.

In particular, the scattering loss increases as the acoustic wavelength decreases [28]. The interface roughness mainly defines the scattering property of sea surface and bottom. High interface roughness induces strong spatial energy dispersion. The roughness of sea surface is due to the capillary waves caused by wind, the amplitude of which ranges from centimeters to meters [10]. The roughness of sea bottom depends on the geology, including, e.g., the roughness of rocks, sand ripples, and organisms in the ground. [3, 10, 26]

In real environments, the two types of scattering processes coexist. For example, in the presence of high wind speed, the wind-generated waves increases the roughness

of sea surface, and breaking waves can create bubble clouds of a large size. Both types of scattering losses happen when the acoustic wave interacts with both sea surface and bubble clouds, and they are modeled as the parameter P_{sl} .

2.2.4 Propagation Loss Parametrization

The parametrization of the propagation loss is accomplished using the information from the previous sections. The attenuation formula model for an acoustic signal at frequency f , the after propagating a distance of ζ can be written as [10]

$$\begin{aligned} P_{att}(f, \zeta) &= P_{sl}P_{gsl}P_{al} \\ &= P_{sl}\zeta^\beta e^{\alpha_{ac}(f)\zeta}, \end{aligned} \quad (2.6)$$

taking the log from both sides yields

$$10 \log(P_{att}(f, \zeta)) = 10 \log(P_{sl}) + 10\beta \log(\zeta) + 10\zeta \alpha_{ac}(f), \quad (2.7)$$

which is a another form of writing the propagation loss [14, 17, 27]. Figure 2.5 shows an example of how the propagation loss behaves as function of frequency and distance. In this example, $\beta = 1.5$ and $P_{sl} = 0.5$.

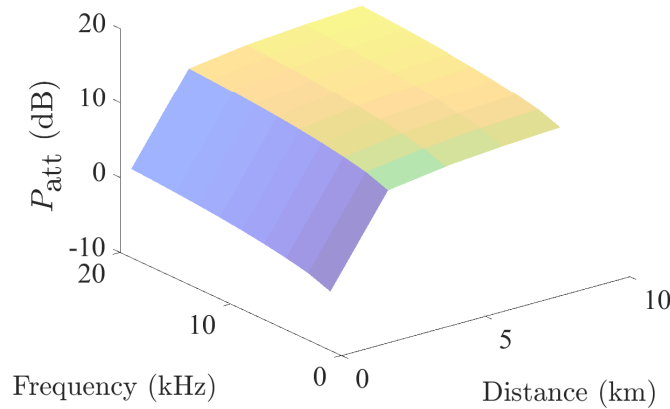


Figure 2.5: Attenuation (dB) in terms of frequency (kHz) and distance (km).

Moreover, differently from the propagation loss in terrestrial radio channel which only has spreading loss with an exponent $2 \sim 6$ [52], the propagation loss in UWA channels is spreading-loss dominant in the near-distance transmission, while in long-distance transmissions the absorption-loss is dominant [10].

2.2.5 Time-Varying Multipath

The acoustic wave propagation affects the communication system in more ways than just with its velocity and its energy loss. In a UWA transmission, the wave goes through multiple paths before reaching the receiver. In a shallow water environment, where the transmission distance is larger than the water depth, wave reflections from the surface and the bottom generate multiple arrivals of the same signal, with different amplitudes and phases. In deep water applications, surface and bottom reflections may be neglected, as illustrated in Figure 2.3b. However, the wave refractions due to the spatially varying sound speed in the deep water scenario also cause significant multipath phenomena.

2.2.5.1 Large Delay Spread

Some peculiarities arise from the multipath characteristic of the UWA transmission, one of them is the large channel delay spread. The channel delay spread is defined as the maximal difference in the times-of-arrival of channel paths,

$$\Delta\tau_{\max} = \max \{|\tau_p - \tau_q|\}, \quad \forall p, q \in \mathbb{N}_+. \quad (2.8)$$

where τ_p and τ_q are the time-varying delay for the p th and q th paths, respectively.

The low speed of acoustic waves and significant multipath phenomena cause large channel delay spread. For example, two physical arrivals that differ 15 meters in path length lead to an arrival time difference of 10 ms (here we assume the propagation speed of sound is 1500 m/s). In shallow water, the typical delay spread is around several tens of milliseconds [10], but occasionally delay spread can be as large as 100 ms [31]. In deep water, the delay spread can be of the order of seconds. For UWA communications, the significant delay spread leads to severe ISI due to the waveform time-dispersion.

2.2.5.2 Large Doppler Spread

Another characteristic of a UWA communication is the large Doppler spread, which comes from the junction of the wave multipath and environment time variability. For example, the direct path without reflections could be very stable, while

the sea surface reflected paths could have time variations produced by the motion of surface waves. The different time variabilities lead to different Doppler scaling effects or Doppler shifts of the transmitted signal. Denote ψ_p as the relative velocity of the p th path, namely the change rate of the propagation length of the p th path. The channel Doppler rate spread is defined as the maximal difference of the Doppler rates of channel paths,

$$\varphi_{\max} = \max \left\{ \frac{|\psi_p - \psi_q|}{c} \right\}, \quad \forall p, q \in \mathbb{N}_+. \quad (2.9)$$

where $c \in \mathbb{R}$ is the sound speed in water. The slow propagation speed of sound introduces large Doppler spread. For example, consider $\psi = 15$ m/s and $f_c = 30$ kHz, $c = 1500$ m/s, and f_c is the system center frequency. The Doppler frequency shift at f_c is given by

$$f_d = \frac{\psi}{c} f_c = 300 \text{ Hz}. \quad (2.10)$$

This frequency shift may be significant in the context of UWA transmission where the systems work in the kHz part of the frequency spectrum.

Furthermore, large Doppler spread results in a reduction in the channel coherence time (the time period when the channel can be viewed as static) or an apparent increase in the rate of channel fluctuation [51]. The large Doppler spread causes severe interference among different frequency components of the signal (also referred to as frequency-spreading).

2.3 Ambient Noise and External Interference

An essential acoustic characteristic of the ocean is its underwater ambient noise. Depending on applications, underwater acoustic noise consists of different components. Specific to the UWA communication system, the acoustic noise can be grouped into two categories: ambient noise and external interference [10].

Ambient noise is one kind of background noise which comes from a myriad of sources. The conventional sources of ambient noise in water include volcanic and seismic activities, turbulence, various human constructions which generate industrial

and mechanical noises (e.g., ships [53], drilling platforms, etc.), and weather processes such as wind-generated waves and rain, thunder, and thermal noise [24, 27]. Due to multiple sources, ambient noise can be approximated as Gaussian but is not white. The effects of these sources, and the properties of the noise they generate depend on many factors including weather, geographical region, time of day, season, and are exhibited in different frequency bands [27]. For short-range acoustic communication, the level of ambient noise may be well below the desired signal. For long- or short-range UWA communication, the noise level would be a limiting factor for communication, the level of ambient noise may be well below the desired signal.

External interference is an interfering signal which is recognizable in the received signal. Corresponding sources include marine animals, ice cracking, and acoustic systems working in the same environment. For example, snapping shrimp in warm water and ice cracking in polar regions generate impulsive interference [54]. Sonar operations could occasionally happen at the same time communications, creating an external interference which is highly structured [55]. Relative to ambient noise, external interferences are neither Gaussian nor white. The presence of this kind of noises may cause highly dynamic link error rate or even link interruption.

It should be noted that the noise is highly frequency-dependent. The noise power spectrum density almost monotonically decreases as frequency increases, until up to about 100 kHz when terminal noise becomes dominant. Thus, when selecting a suitable frequency band for communication, besides the frequency-dependent path loss as shown in (2.6), noise should also be taken into account [28, 56, 51].

Finally, Figure 2.6 shows a *power spectral density* (PSD) estimation of the transmitted and received signal from a practical transmission made in Arraial do Cabo, RJ ($22^{\circ}58'38.2''\text{S}$, $42^{\circ}01'10.4''\text{W}$) [57]. The sampling frequency was 96 kHz and the distance between transmitter and receiver was 250 m. The original signal, Figure 2.6a, is centered at 7.5 kHz. It is possible to see the effects of the UWA channel in this transmission.

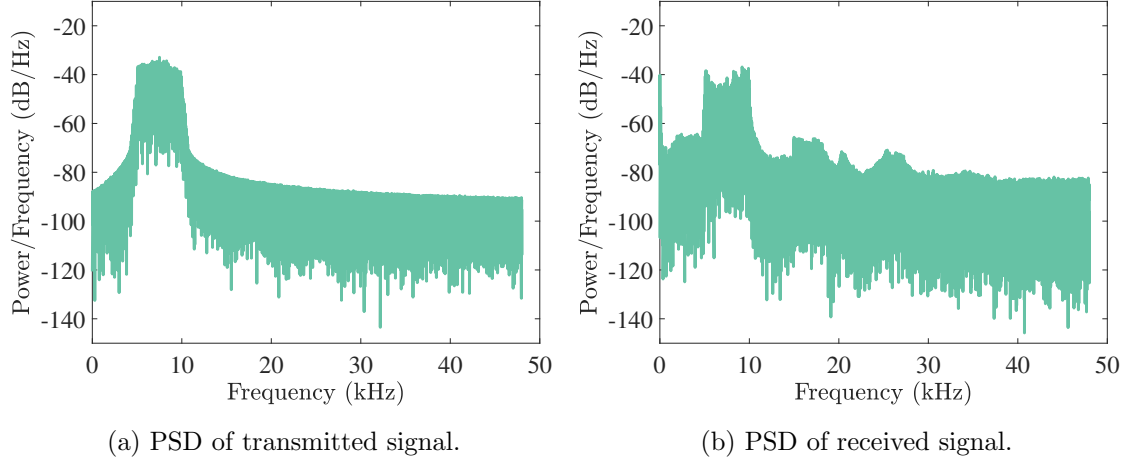


Figure 2.6: Power spectral density estimates of transmitted and received signals of a practical transmission experiment.

Furthermore, to understand better the UWA channel characteristics, modeling the the channel mathematically helps to know it better. Chapter 3 provides a UWA channel input-output relationship that helps to understand the channel, where different assumptions are made to cover different situations where the channel model can be employed.

Chapter 3

Communication System Model

The underwater environment characteristics described in Chapter 2 introduce challenges for the creation of new communication systems. Novel systems must mitigate environment impairments in order to obtain high data throughput. This chapter presents a communication system design, regarding transmitter, receiver, and channel model. The communication system model presented is tested through simulations in Chapter 5 and its performance is evaluated.

3.1 Transceiver Structure Overview

A definition of transceiver is a scheme comprising both a transmitter and receiver. In this sense, Figure 3.1 shows a transceiver structure that represents the communication system model employed in this project. Each part is responsible for enabling the system to mitigate the impairments described in Chapter 2. The first impairment studied in this work is ISI, which is the leading cause of high BER in UWA communication systems. Thus, a solution to the ISI problem is to design a receiver that employs a mechanism called equalizer for compensating or reducing the ISI in the received signal. Because the equalization is the center on this work, Chapter 4 is dedicated entirely to the study of equalizers, and the presented structured is adjusted to permit the iterations of the turbo equalization. Moreover, this chapter describes the remainder of the system in Figure 3.1. Each component is presented, and its influences on the UWA communication system are discussed.

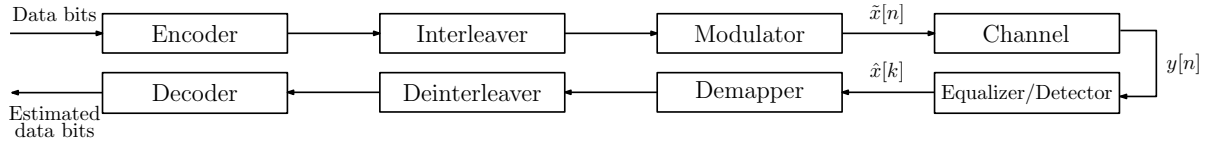


Figure 3.1: Illustration of the transceiver structure.

3.2 Transceiver Description

This section describes each part of the transceiver. Blocks from the transmitter and the receiver are analyzed together when it simplifies the interpretation, e.g., Interleaver and Deinterleaver.

3.2.1 Information Source

Any information source, considering it to be the output of a source encoder, not depicted in Figure 3.1 to simplify the transceiver structure, produces an output that can be a *random variable* (RV), i.e., the data bits input on the Encoder block are characterized in statistical terms. Otherwise, if the information source output were known precisely (being deterministic), there would be no need to transmit it [58]. It is assumed here that the Encoder block input sequence is statistically independent. That is, the current input is statistically independent of all past and future outputs. The bits that enter the Encoder are considered to be sampled from a uniform distribution, which in practical applications the assumption may not be realistic. However, the use of interleaver and redundant bits help to ensure this assumption.

3.2.2 Encoder & Decoder

The type of *forward error correction* (FEC) or channel encoding technique used in this work is called *convolutional code*, which was first introduced by Elias in 1955 [59]. He showed that redundancy can be introduced into a data stream through the use of linear shift registers. He also showed that the resulting codes were very good when randomly chosen. This result was very interesting, because of its correlation with Shannon's more theoretical work, showing that there exist randomly selected codes that, on the average, provide arbitrarily high levels of reliability for a given

data transmission at a rate less than the channel capacity [60].

Figure 3.2 shows an 1/3-rate linear convolutional encoder. The rate is established by the fact that the encoder outputs three bits for every input bit. In general, an encoder with θ inputs and ϱ outputs is said to have rate θ/ϱ [61, 62]. In Figure 3.2, a binary data stream, represented as Input is fed into a shift-register circuit consisting of a series of memory elements. At each successive input to the shift register, the values of the memory elements are tapped off and added according to a fixed pattern, creating in this example, three outputted bits. The output from the terminations can be multiplexed in various ways, creating a diversity of stream patterns.

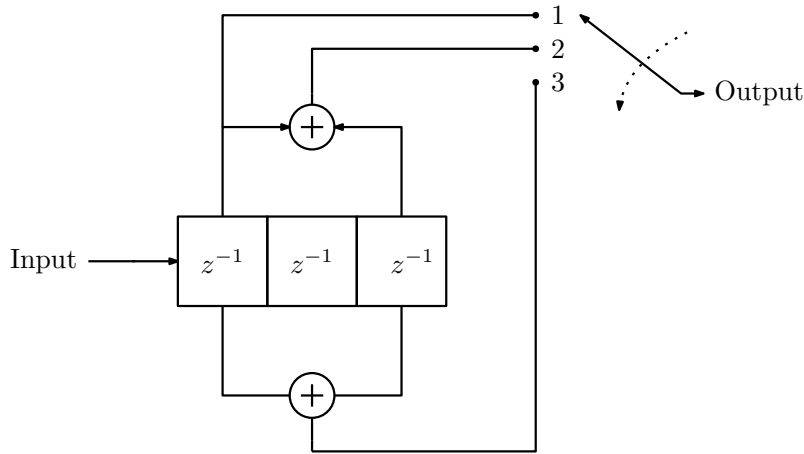


Figure 3.2: An 1/3-rate, $K = 3$ linear convolutional encoder.

Along with the previously mentioned rate of the code and memory, the constraint length is another characteristic that distinguishes a convolutional encoder from each other. The constraint length K of a convolutional code is the maximum number of bits in a single output stream that can be affected by any input bit, which is also the maximum number of taps on the shift registers in the encoder circuit.

A convolutional encoder can be seen as a finite-state machine. Hence the optimum decoder is a *maximum likelihood sequence estimator* (MLSE). The MLSE makes its decision on observation of a sequence of received signals over successive signal intervals. The optimum decoding of a convolutional code involves a search through the trellis for the most probable sequence. Depending on whether the detector

following the demodulator performs hard or soft decisions, the corresponding metric in the trellis search may be either a Hamming metric or an Euclidean metric [63].

We are not going into details here, but the algorithm may reduce the number of sequences in the trellis search, eliminating sequences as new data are received from the deinterleaver. Details about the metrics and procedure can be seen at [35, 58, 64].

3.2.3 Interleaver & Deinterleaver

Error-correcting codes can correct errors successfully as long as there are not too many errors in a single codeword. However, errors sometimes tend to happen in bursts, in the sense that there can be a local concentration of affected data [65]. Channels characterized by multipath, as the UWA channel, exhibit bursty error characteristics. Signal fading due to time-variant multipath propagation often causes the signal to fall below the noise level, thus resulting in a large number of errors. Such error clusters are not usually corrected by codes that are optimally designed for statistically independent errors. An effective method for dealing with burst error channels is to interleave the coded data in such a way that the bursty channel is transformed into a channel having independent errors. Thus, a code designed for independent channel errors is used. An interleaver is a device that mixes up the symbols from several code words so that the symbols from any given code word are well separated during transmission [35]. In Figure 3.3, the bits are inputted row-wise and outputted column-wise. This is an example of how to construct a interleaver. When the code words are reconstructed by the deinterleaver, error bursts introduced by the channel are broken up and spread across several code words. The interleaver/deinterleaver pair creates an effectively random channel [58].

In this project, a random block interleaver is employed, which chooses a permutation table randomly using an initial seed parameter. By using the same initial seed value in the corresponding random deinterleaver block, it is possible to restore the permuted symbols to their original ordering.

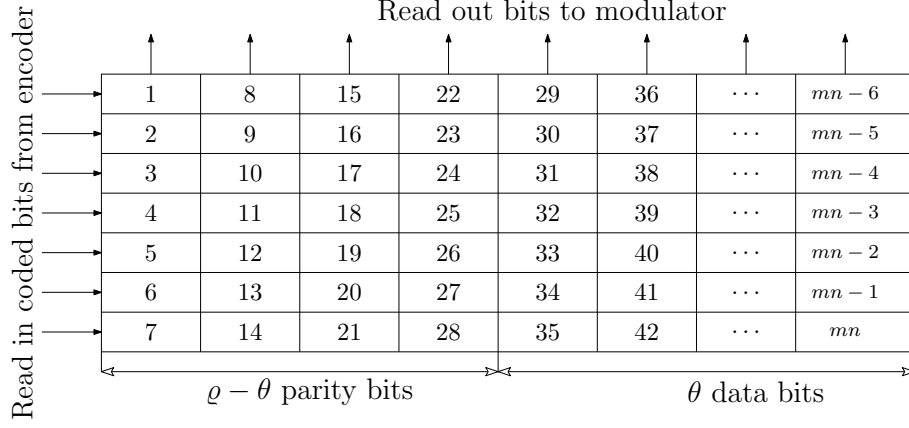


Figure 3.3: Example of block interleaver where data is inputted row-wise and read column-wise.

3.2.4 Modulator & Demodulator

A modulator converts an input sequence of bits into a waveform suitable for transmission over a communication channel [64]. The modulator (demodulator analogously) can be described in three separate parts as illustrated in Figure 3.4. Note that, in contrast with Figure 3.1, the Equalizer block is not depicted after the Waveform to Signals block for simplicity and Detector block is comprised by the Passband to Baseband and Waveform to Signals blocks. The basic parts of a modulator will then turn out to be a procedure for mapping a sequence of binary digits into a sequence of real or complex numbers, followed by the mapping of a sequence of numbers into a waveform. The last part maps a baseband waveform into a bandpass waveform. At the demodulator, the bandpass waveform is mapped back to baseband before the other components of demodulation¹ are performed.

The modulation process is performed as follows. The interleaved bits are mapped into constellation signals, e.g, M -PSK digital modulation [35] and then converted into a waveform. Consider the mapped signal $x[k] \in \mathcal{C} \subset \mathbb{C}$, signal of a generic constellation \mathcal{C} and with sampling period $T \in \mathbb{R}_+$. In order to be transmitted, this signal has to be converted in a waveform first. The first step is the upsampling

¹Note that this frequency conversion operation is often referred to as modulation and demodulation, but is more common today to use the word modulation/demodulation for the entire process of mapping bits to waveforms and the reverse process [64].

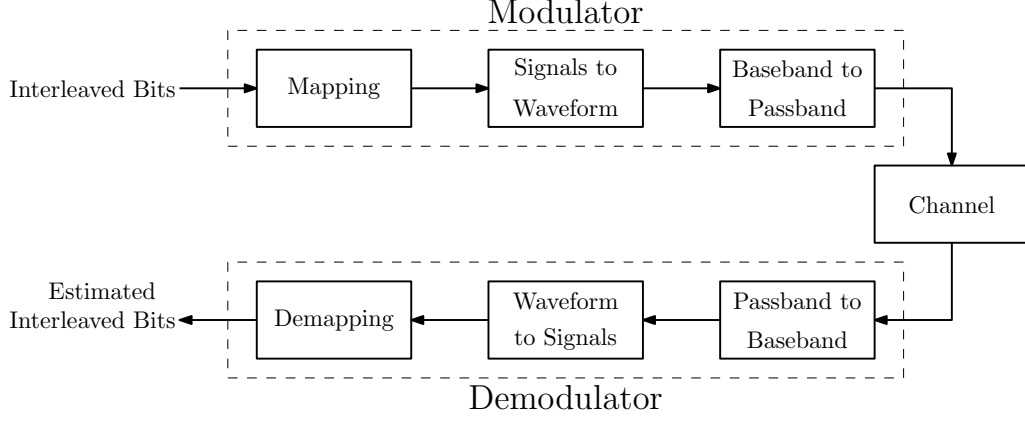


Figure 3.4: Illustration of modulator and demodulator structure.

operation by a factor Q , this operation yields the new signal given by

$$x_a[n] = \sum_{k \in \mathcal{K}} x[k] \delta[n - kQ], \quad (3.1)$$

where $\mathcal{K} = \{1, 2, \dots, K\}$ is the set containing all the time indexes. After upsampling, the signal is then mapped into a waveform $x_b[n]$ through a convolution with a basic pulse waveform $p[n]$. This operation is known as pulse shaping, and the pulse waveform $p[n]$ can be chosen so that in a transmission absent of multipath it would result in no ISI. Waveforms with the desired properties for $p[n]$ are said to be ideal Nyquist [64]. The pulse shaping operation can be written as

$$\begin{aligned} x_b[n] &= x_a[n] * p[n] \\ &= \sum_{k \in \mathcal{K}} x[k] p[n - kQ]. \end{aligned} \quad (3.2)$$

Then, the signal is upconverted to bandpass to be transmitted, yielding

$$\tilde{x}[n] = 2\Re \{ x_b[n] e^{j2\pi f_c n} \} \quad (3.3)$$

$$= x_b[n] e^{j2\pi f_c n} + x_b^*[n] e^{-j2\pi f_c n}. \quad (3.4)$$

At the receiver, the demodulator does the inverse process done at the modulator, which results in estimates of the interleaved bits, because of channel impairments on the transmitted signal. The process done at the receiver will be explained in details in Section 3.4.

3.3 Channel

This section evolves around the Channel block in Figure 3.1. The UWA channel input-output relationship is explored, including how the Doppler effect impacts the models.

3.3.1 UWA Channel Input-Output Relationship

A diagram for the UWA communication system analog front-end in the presence of a UWA channel is shown in Figure 3.5. The digital front-end part, not represented in the illustration, provides to the analog front-end the bandpass samples $\tilde{x}[n]$. The samples are then converted into an analog signal $\tilde{x}(t)$ by the *digital-to-analog convert* (DAC), which is amplified, and passed to the matching circuits. The signal goes through the UWA channel and gets to the receiver. Moreover, at the receiver side, the signal that suffered attenuation throughout the UWA channel is preamplified. Then the signal is filtered by a bandpass filter in order to remove interference from outside the desired bandwidth and sampled at the bandpass. All the modules in Figure 3.5 between $\tilde{x}(t)$ and $\tilde{y}(t)$ are what is called channel in this work, comprised one block in Figure 3.1.

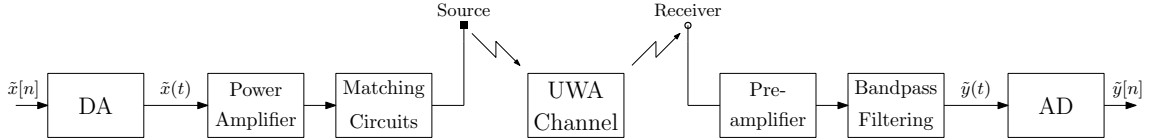


Figure 3.5: UWA communication system analog front-end.

The channel input-output relationship is established directly in the bandpass. This model allows the capture of the wideband channel effect, such as: the propagation effect is frequency-dependent, each transducer has its transmit voltage response, and the matching is not uniform in the signal band, and the Doppler distortion is frequency dependent.

Assume that the *channel impulse response* (CIR) is a linear and time-varying system. Then, we can represent it by $\tilde{h}(t, \tau)$. From the signal processing perspective,

the overall bandpass channel between the transmitter and the receiver is

$$\begin{aligned}\tilde{y}(t) &= \tilde{x}(t) * \tilde{h}(t, \tau) + \tilde{v}(t) \\ &= \int \tilde{h}(t, \tau) \tilde{x}(t - \tau) d\tau + \tilde{v}(t),\end{aligned}\tag{3.5}$$

where $\tilde{v}(t)$ is the bandpass noise at the receiver.

The CIR $\tilde{h}(t, \tau)$ is general with no specified structure. From the system identification point of view, we need to parameterize the channel. The next Sections are going to model the channel $\tilde{h}(t, \tau)$ under different assumptions.

3.3.2 Linear Time-varying Channel with Path-specific Doppler Scales

In order to parameterize the channel $h(t, \tau)$, the starting point is the assumption that the channel consists of P discrete paths.

$$\tilde{h}(t, \tau) = \sum_{p \in \mathcal{P}} a_p(t) \delta(\tau - \tau_p(t)), \quad \forall p \in \mathcal{P} = \{1, 2, \dots, P\} \tag{3.6}$$

where $a_p(t) \in \mathbb{R}_+$ and $\tau_p(t) \in \mathbb{R}_+$ are the time-varying amplitude and delay for the p th path, respectively, and $\delta(t)$ is the Dirac delta function, which is zero everywhere except at the origin, where it is infinite,

$$\delta(t) = \begin{cases} \infty, & t = 0 \\ 0, & t \neq 0 \end{cases}, \tag{3.7}$$

and which is also constrained to satisfy the identity:

$$\int_{-\infty}^{+\infty} \delta(t) dt = 1. \tag{3.8}$$

For a short block of length T_{bl} period, one can assume that $a_p(t)$ and $\tau_p(t)$ as slowly varying. For this, one can adopt two assumptions. The first is that the amplitude is constant within a short block, $a_p(t) = a_p$. The second is that the delay variation within one block can be approximated by a first order polynomial

$$\tau_p(t) \approx \tau_p - \varphi_p t \quad t \in [0, T_{\text{bl}}], \tag{3.9}$$

where $\tau_p \in \mathbb{R}_+$ is the initial delay and $-\varphi_p \in \mathbb{R}$ is the first order derivative of $\tau_p(t)$.

The parameter φ_p is often termed the Doppler scaling factor. Based on the assumptions, we have a time varying channel with different Doppler scales on different paths as

$$\tilde{h}(t, \tau) = \sum_{p \in \mathcal{P}} a_p \delta(\tau - (\tau_p - \varphi_p t)) \quad t \in [0, T_{\text{bl}}]. \quad (3.10)$$

The received bandpass signal is related to the transmitted bandpass signal as

$$\tilde{y}(t) = \sum_{p \in \mathcal{P}} a_p \tilde{x}((1 + \varphi_p)t - \tau_p) + \tilde{v}(t) \quad (3.11)$$

where the equivalent bandpass noise $\tilde{v}(t)$, which contains both ambient and model-mismatch noises.

Equation (3.10) gives us a channel model that is possible to represent each path with specific Doppler scale. However, it is reasonable to assume that the Doppler scale might be constant to in specific scenarios. Thus, the next Section presents a channel model under the assumption of invariability of the Doppler scale among paths.

3.3.3 Linear Time-varying Channel with One Common Doppler Scale

Assume that all the paths have the same Doppler scale factor, where the $\varphi_p = \varphi$ is a constant. The channel is simplified to

$$\tilde{h}(t, \tau) = \sum_{p \in \mathcal{P}} a_p \delta(\tau - (\tau_p - \varphi t)) \quad t \in [0, T_{\text{bl}}]. \quad (3.12)$$

From the assumption that all the paths are stable with no delay variation, it is possible to derive a more specific channel model, a *linear time-invariant* (LTI) channel combined with a resampling operation in the transmitted signal.

This can be derive as shown in [66]. Assume that all the paths are stable with no delay variation, the received bandpass signal can be written as

$$\begin{aligned}
\tilde{y}(t) &= \sum_{p \in \mathcal{P}} a_p \tilde{x}((1 + \varphi)(t - \tau_p/(1 + \varphi))) \int_{-\infty}^{+\infty} \delta(\tau - \tau_p/(1 + \varphi)) d\tau + \tilde{v}(t) \\
&= \int_{-\infty}^{+\infty} \sum_{p \in \mathcal{P}} a_p \delta(\tau - \tau_p/(1 + \varphi)) \tilde{x}((1 + \varphi)(t - \tau)) d\tau + \tilde{v}(t) \\
&= \int_{-\infty}^{+\infty} \tilde{h}(\tau) \tilde{x}((1 + \varphi)(t - \tau)) d\tau + \tilde{v}(t) \\
&= \tilde{h}(t) * \tilde{x}((1 + \varphi)t) + \tilde{v}(t), \quad t \in [0, T_{bl})
\end{aligned} \tag{3.13}$$

where

$$\tilde{h}(t) = \sum_{p \in \mathcal{P}} a_p \delta(t - \bar{\tau}_p), \tag{3.14}$$

represents the CIR and $\bar{\tau}_p = \tau_p/(1 + \varphi)$ is the new delay related to the p th path.

Equation (3.13) shows that $\tilde{y}(t)$ can be written as a convolution between the LTI channel and the transmitted signal scaled by the Doppler scaling factor. Then, a regular Doppler scale can be readily removed through a rescaling operation [10].

3.3.4 Linear Time-invariant Channel

Further simplification on the CIR model can be done by setting $\varphi = 0$, hence $\bar{\tau}_p = \tau_p$. This models a transmission condition where the Doppler effect can be overlooked. Then, the LTI CIR is given by

$$\tilde{h}(t) = \sum_{p \in \mathcal{P}} a_p \delta(t - \tau_p). \tag{3.15}$$

3.3.5 Digital Implementation

To implement the UWA CIR used for the equalizers discussed in Chapter 4 and for the proposed simulations in Chapter 5, it is necessary to sample the equation (3.15) with a T_a sampling period ². On the discrete model, each τ_p is mapped to a η_p following

$$\eta_p = \left\lceil \frac{\tau_p}{T_a} \right\rceil, \tag{3.16}$$

then, as showed in Figure 3.6.

² T_a is given by QT .

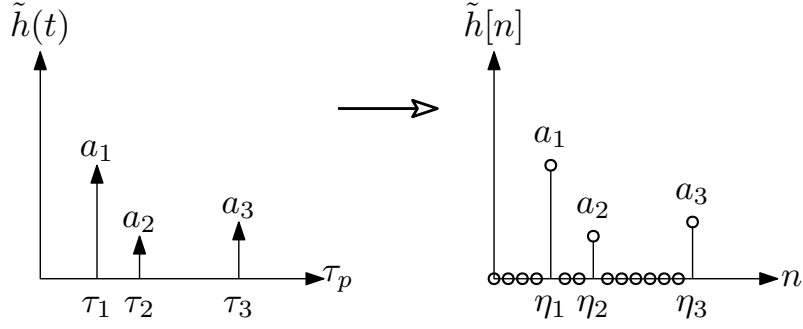


Figure 3.6: Example of sampling of LTI CIR.

Then, the discrete representation of CIR is written as follows

$$\tilde{h}[n] = \sum_{l \in \mathcal{L}} h_l \delta[n - l], \quad (3.17)$$

where $\mathcal{L} = \{1, 2, \dots, \eta_1, \eta_1 + 1, \dots, \eta_2, \dots, \eta_P\}$, and

$$h_l = \begin{cases} a_p, & \text{if } l = \eta_p \\ 0, & \text{otherwise} \end{cases}.$$

The parameter τ_p is calculated given the difference between the delay of each path, $\Delta\tau_p$. This parameter $\Delta\tau_p$ follows an exponential distribution with mean $\Delta\tau_m$ and each τ_p is given by

$$\tau_p = \sum_{i=1}^p \Delta\tau_i. \quad (3.18)$$

In a CIR, for each path, it is necessary to generate different values of $\Delta\tau_p$ and then use (3.18) to compute τ_p .

Moreover, each path amplitude a_p is determined by a probability distribution. There is no consensus in the literature for the best fitting distribution for the gain, considered to vary according to the bathymetric profile. Some common distributions used are Rayleigh [67], Rice [68, 69], log-normal [70], K-distribution [71], and Beta-Nakagami [72].

3.4 Baseband Signal Model

Assuming full knowledge of the CIR $\tilde{h}[n]$ given by equation (3.17) and given the $\tilde{x}[n]$ from equation (3.3), it is possible to model the reception as convolution between

both and an additive noise. The bandpass digital received signal is given by

$$\begin{aligned}\tilde{y}[n] &= \tilde{h}[n] * \tilde{x}[n] + \tilde{v}[n] \\ &= \sum_{l \in \mathcal{L}} h_l[n] \tilde{x}[n-l] + \tilde{v}[n]\end{aligned}\tag{3.19}$$

where $\tilde{y}[n]$ is a realization of the RV $\tilde{Y}[n]$ that models the received signal, $\tilde{x}[n]$ is a realization of the RV $\tilde{X}[n]$ that models the transmitted signal, and $\tilde{v}[n]$ is a realization of the RV $\tilde{V}[n]$ that models the additive noise. As the signal processing at the receiver is done in baseband, it is convenient to write (3.19) as its baseband equivalent signal model given by

$$\begin{aligned}y_b[n] &= \text{LPF} \left\{ \tilde{y}[n] e^{-j2\pi f_c n} \right\} \\ &= \text{LPF} \left\{ \left(\sum_{l \in \mathcal{L}} h_l \tilde{x}[n-l] + \tilde{v}[n] \right) e^{-j2\pi f_c n} \right\} \\ &= \text{LPF} \left\{ \sum_{l \in \mathcal{L}} h_l e^{-j2\pi f_c n} \tilde{x}[n-l] + \tilde{v}[n] e^{-j2\pi f_c n} \right\} \\ &= \text{LPF} \left\{ \sum_{l \in \mathcal{L}} h_l e^{-j2\pi f_c n} \tilde{x}[n-l] \right\} + v_b[n],\end{aligned}\tag{3.20}$$

where $\text{LPF} \{ \cdot \}$ is a low-pass filter operation. Using (3.4), (3.20) can be rewritten as

$$\begin{aligned}y_b[n] &= \text{LPF} \left\{ \sum_{l \in \mathcal{L}} h_l e^{-j2\pi f_c n} (x_b[n-l] e^{j2\pi f_c n} + x_b^*[n-l] e^{-j2\pi f_c n}) \right\} + v_b[n] \\ &= \text{LPF} \left\{ \sum_{l \in \mathcal{L}} h_l e^{-j2\pi f_c l} x_b[n-l] \right\} + \text{LPF} \left\{ \sum_{l \in \mathcal{L}} h_l e^{-j4\pi f_c n-l} x_b^*[n-l] \right\} + v_b[n].\end{aligned}\tag{3.21}$$

Considering an ideal *low-pass filter* (LPF), the second term in equation (3.21) is outside the filter's bandpass, yielding

$$\begin{aligned}y_b[n] &= \sum_{l \in \mathcal{L}} h_l e^{-j2\pi f_c l} x_b[n-l] + v_b[n] \\ &= \left(\underbrace{\sum_{l \in \mathcal{L}} h_l e^{-j2\pi f_c l} \delta[n-l]}_{h_b[n]} \right) * x_b[n] + v_b[n].\end{aligned}\tag{3.22}$$

Then, applying the matched filter to the pulse shaping, the following holds

$$\begin{aligned}
y[n] &= p[\eta - n] * y_b[n] \\
&= p[\eta - n] * h_b[n] * x_b[n] + p[\eta - n] * v_b[n] \\
&= \underbrace{(p[\eta - n] * h_b[n] * p[n])}_{h[n]} * \left(\sum_{k \in \mathcal{K}} x[k] \delta[n - kQ] \right) + p[\eta - n] * v_b[n] \\
&= \sum_{k \in \mathcal{K}} x[k] h[n - kQ] + v[n] \\
&= h[n] * x[n] + v[n],
\end{aligned} \tag{3.23}$$

where $\eta \in \mathbb{N}$ is the delay introduced by the signal processing in the transmitter and the channel.

Equation (3.23) represents the upsampled baseband version of the received signal. For the signal processing at the receiver, the received signal is downsampled by Q in order to work at the same sampling frequency as the baseband signal in the transmitter. Therefore, the downsampled version is

$$y[k] = h[k] * x[k] + v[k], \tag{3.24}$$

where $y[k]$ is a realization of the RV $Y[k]$ that models the baseband received signal, $x[k]$ is a realization of the RV $X[k]$ that models the baseband transmitted signal, and $v[k]$ is a realization of the *additive white Gaussian noise* (AWGN) RV $V[k]$.

Then, in its matrix form the baseband-equivalent equation can be written as

$$\mathbf{y} = \mathbf{H}\mathbf{x} + \mathbf{v}, \tag{3.25}$$

where $\mathbf{y} \in \mathbb{C}^{N \times 1}$ is a realization of a random vector $\mathbf{y} = [Y[1], Y[2], \dots, Y[N]]^T$ that models the baseband received signal vector; $\mathbf{x} \in \mathbb{C}^{K \times 1}$ is a realization of a random vector $\mathbf{x} = [X[1] X[2] \dots X[K]]^T$, which models the transmitted signal, $\mathbf{v} \in \mathbb{C}^{N \times 1}$ is a realization of the AWGN a random vector $\mathbf{v} \sim \mathcal{CN}(\mathbf{0}_{N \times 1}, \sigma_V^2 \mathbf{I}_N)$, and

$\mathbf{H} \in \mathbb{C}^{N \times K}$ is the Toeplitz channel matrix, that can be written as

$$\mathbf{H} = \begin{bmatrix} h_1 & 0 & \cdots & 0 & 0 \\ h_2 & h_1 & \cdots & 0 & 0 \\ \vdots & \vdots & \cdots & \vdots & \vdots \\ h_L & h_{L-1} & \cdots & 0 & 0 \\ 0 & h_L & \cdots & 0 & 0 \\ \vdots & \vdots & \ddots & \vdots & \vdots \\ 0 & 0 & \cdots & h_{L-1} & h_{L-2} \\ 0 & 0 & \cdots & h_L & h_{L-1} \\ 0 & 0 & 0 & \cdots & h_L \end{bmatrix}, \quad (3.26)$$

where $N = K + L - 1$.

The UWA multipath channel induces ISI, which degrades the quality of the received signal. Thus, in order to recover the original message, the receiver must equalize the received signal to mitigate the effects of the channel. The estimated signal $\hat{\mathbf{x}}$ is given by

$$\hat{\mathbf{x}} = \mathbf{W}\mathbf{H}\mathbf{x} + \mathbf{W}\mathbf{v}. \quad (3.27)$$

where $\mathbf{W} \in \mathbb{C}^{K \times N}$ is the equalization matrix. Equalization techniques are going to be discussed in Chapter 4.

3.5 Channel Estimation

In the previous section, it was assumed full knowledge of the CIR, where in a practical scenario, the receiver does not have full knowledge of the channel. Thus, it is necessary to estimate the CIR, the usual way to perform this task is using pilots in the transmission. The pilots are a set of signals that are known both at transmitter and receiver. To perform the CIR estimation in this work, the reception is modeled as linear convolution ignoring the effect of the AWGN, reducing the estimation to a least-squares problem. This model is given by

$$\mathbf{y} = \mathbf{H}\boldsymbol{\phi}, \quad (3.28)$$

where $\boldsymbol{\phi} \in \mathbb{C}^{K \times 1}$ is the pilot vector. By the linear property of convolution, equation (3.28) can be rewritten with $\boldsymbol{\phi}$ in a Toeplitz matrix form $\boldsymbol{\Phi} \in \mathbb{C}^{N \times K}$

$$\mathbf{y} = \boldsymbol{\Phi} \mathbf{h}, \quad (3.29)$$

where $\mathbf{h} \in \mathbb{C}^{K \times 1}$ is the CIR. Equation (3.29) can be solved using least-squares, where it minimizes the squared error between \mathbf{y} and $\boldsymbol{\Phi} \mathbf{h}$. The least-squares solution of equation (3.29) is given by

$$\hat{\mathbf{h}} = (\boldsymbol{\Phi}^H \boldsymbol{\Phi})^{-1} \boldsymbol{\Phi}^H \mathbf{y}. \quad (3.30)$$

This estimated CIR $\hat{\mathbf{h}} \in \mathbb{C}^{K \times 1}$ is used on the simulations presented in Chapter 5.

Chapter 4

Equalizers

As described in Chapter 2, the UWA channel can be very challenging. The message received may be corrupted and deviate from what was transmitted, and impairments such as the ISI are responsible for this behavior. Chapter 3 shows what the communication system would do to mitigate the channel effects, and the current chapter is focused in one specific mechanism to enhance reception success, the equalization process. Four different equalizers are going to be discussed, the ZFE, the MMSEE, the DFE, and the TEQ. Each one has its characteristics, with its performance evaluated in terms of BER latter in this work. The first one to be described is the ZFE.

4.1 Zero-forcing Equalizer

The ZFE is a solution for mitigating the ISI that tries to restore the Nyquist Criterion for a free ISI transmission by inverting the channel matrix [73, 74]. The “zero-forcing” term means that the aim is to force the residual ISI to zero. The ZFE overlooks the additive noise, and solves the least squares problem $\mathbf{y} = \mathbf{H}\mathbf{x}$, minimizing the squared difference between the received signal \mathbf{y} and $\mathbf{H}\mathbf{x}$, where \mathbf{H}

is the channel matrix and \mathbf{x} the transmitted signal [75]. Then, the following holds

$$\begin{aligned}
\xi(\mathbf{x}) &= \|\mathbf{y} - \mathbf{H}\mathbf{x}\|_2^2 \\
&= (\mathbf{y} - \mathbf{H}\mathbf{x})^H (\mathbf{y} - \mathbf{H}\mathbf{x}) \\
&= (\mathbf{y}^H - \mathbf{x}^H \mathbf{H}^H) (\mathbf{y} - \mathbf{H}\mathbf{x}) \\
&= \mathbf{y}^H \mathbf{y} - \mathbf{y}^H \mathbf{H}\mathbf{x} - \mathbf{x}^H \mathbf{H}^H \mathbf{y} + \mathbf{x}^H \mathbf{H}^H \mathbf{H}\mathbf{x} \\
&= \mathbf{y}^H \mathbf{y} - 2\mathbf{y}^H \mathbf{H}\mathbf{x} + \mathbf{x}^H \mathbf{H}^H \mathbf{H}\mathbf{x}.
\end{aligned} \tag{4.1}$$

Minimizing (4.1) by $\partial\xi(\mathbf{x})/\partial\mathbf{x}^* = 0$

$$\begin{aligned}
\frac{\partial\xi(\mathbf{x})}{\partial\mathbf{x}^*} &= 0 \Rightarrow \\
2\mathbf{H}^H \mathbf{y} + 2\mathbf{H}^H \mathbf{H}\mathbf{x} &= 0 \\
\mathbf{H}^H \mathbf{H}\mathbf{x} &= \mathbf{H}^H \mathbf{y}.
\end{aligned} \tag{4.2}$$

Therefore, the estimated data block $\hat{\mathbf{x}}$ is given by

$$\hat{\mathbf{x}} = (\mathbf{H}^H \mathbf{H})^{-1} \mathbf{H}^H \mathbf{y}, \tag{4.3}$$

whereas the ZFE matrix is

$$\mathbf{W}_{\text{ZF}} = (\mathbf{H}^H \mathbf{H})^{-1} \mathbf{H}^H. \tag{4.4}$$

One of the drawbacks regarding this equalizer is ignoring the effect of additive noise when modeling the problem as $\mathbf{y} = \mathbf{H}\hat{\mathbf{x}}$, which may lead to overall performance degradation due to noise enhancement.

4.2 Minimum Mean Square Error Equalizer

A solution to overcome the noise enhancement caused by the ZFE is the use of MMSEE [36], which takes into account the additive noise for data block estimation. The *mean square error* (MSE) between the transmitted and estimated data blocks is used to derive the equalizer coefficients. Thus, the MMSEE matrix [76] is solution of the following convex optimization problem

$$\begin{aligned}
&\underset{\mathbf{W} \in \mathbb{C}^{N \times M}}{\text{minimize}} \xi(\mathbf{W}) = \mathbb{E} \{ \|\mathbf{x} - \hat{\mathbf{x}}\|_2^2 \} \\
&\text{subject to } \mathbf{W}\mathbf{y} = \hat{\mathbf{x}}
\end{aligned} \tag{4.5}$$

The problem given by (4.5) has an exact solution, that can be derive as the following.

$$\begin{aligned}
\xi(\mathbf{W}) &= \mathbb{E} \left\{ \|\mathbf{x} - \mathbf{W}(\mathbf{H}\mathbf{x} + \mathbf{v})\|_2^2 \right\} \\
&= \mathbb{E} \left\{ (\mathbf{x} - \mathbf{W}(\mathbf{H}\mathbf{x} + \mathbf{v}))^H (\mathbf{x} - \mathbf{W}(\mathbf{H}\mathbf{x} + \mathbf{v})) \right\} \\
&= \text{Tr} \left\{ \mathbb{E} \left\{ (\mathbf{x} - \mathbf{W}(\mathbf{H}\mathbf{x} + \mathbf{v})) (\mathbf{x} - \mathbf{W}(\mathbf{H}\mathbf{x} + \mathbf{v}))^H \right\} \right\} \\
&= \text{Tr} \left\{ \mathbb{E} \{ \mathbf{x}\mathbf{x}^H \} - \mathbb{E} \{ \mathbf{x}\mathbf{x}^H \} \mathbf{H}^H \mathbf{W}^H - \mathbb{E} \{ \mathbf{x}\mathbf{v}^H \} \mathbf{W}^H - \mathbf{W} \mathbb{E} \{ \mathbf{x}\mathbf{x}^H \} \right. \\
&\quad + \mathbf{W} \mathbb{E} \{ \mathbf{x}\mathbf{x}^H \} \mathbf{H}^H \mathbf{W}^H + \mathbf{W} \mathbb{E} \{ \mathbf{x}\mathbf{v}^H \} \mathbf{W}^H - \mathbf{W} \mathbb{E} \{ \mathbf{v}\mathbf{x}^H \} \\
&\quad \left. + \mathbf{W} \mathbb{E} \{ \mathbf{v}\mathbf{x}^H \} \mathbf{H}^H \mathbf{W}^H + \mathbf{W} \mathbb{E} \{ \mathbf{v}\mathbf{v}^H \} \mathbf{W}^H \right\}, \tag{4.6}
\end{aligned}$$

The assumptions made on Chapter 3 with respect to the transmitted symbol block and noise distributions imply that $\mathbb{E} \{ \mathbf{v}\mathbf{v}^H \} = \sigma_V^2 \mathbf{I}_N$, $\mathbb{E} \{ \mathbf{x}\mathbf{v}^H \} = \mathbb{E} \{ \mathbf{x} \} \mathbb{E} \{ \mathbf{v} \}^H = \mathbf{0}_{K \times N}$. Moreover, assuming that $\mathbf{x} \sim \mathcal{CN}(\mathbf{0}_{K \times 1}, \sigma_X^2 \mathbf{I}_K)$, $\mathbb{E} \{ \mathbf{x}\mathbf{x}^H \} = \sigma_X^2 \mathbf{I}_K$. Thus, (4.6) can be written as

$$\xi(\mathbf{W}) = \text{Tr} \left\{ \sigma_X^2 \mathbf{I}_K - \sigma_X^2 \mathbf{H}^H \mathbf{W}^H - \sigma_X^2 \mathbf{W} \mathbf{H} + \sigma_X^2 \mathbf{W} \mathbf{H} \mathbf{H}^H + \sigma_V^2 \mathbf{W} \mathbf{W}^H \right\}. \tag{4.7}$$

Minimizing (4.7) by $\partial J(\mathbf{W}_{\text{MMSE}})/\partial \mathbf{W}^* = 0$, then

$$\frac{\partial \xi(\mathbf{W}_{\text{MMSE}})}{\partial \mathbf{W}^*} = \sigma_X^2 \mathbf{W}_{\text{MMSE}} \mathbf{H} \mathbf{H}^H - \sigma_X^2 \mathbf{H}^H + \sigma_V^2 \mathbf{W}_{\text{MMSE}} = 0. \tag{4.8}$$

The estimated data block $\hat{\mathbf{x}}$ becomes

$$\hat{\mathbf{x}} = \left(\mathbf{H}^H \mathbf{H} + \frac{\sigma_V^2}{\sigma_X^2} \mathbf{I}_N \right)^{-1} \mathbf{H}^H \mathbf{y}, \tag{4.9}$$

where the MMSEE matrix is

$$\mathbf{W}_{\text{MMSE}} = \left(\mathbf{H}^H \mathbf{H} + \frac{\sigma_V^2}{\sigma_X^2} \mathbf{I}_N \right)^{-1} \mathbf{H}^H. \tag{4.10}$$

There are similarities between the expressions for computing the MMSEE and the ZFE. In high *signal-to-noise ratio* (SNR) regime, \mathbf{W}_{MMSE} is close to \mathbf{W}_{ZF} . Alternatively, this can be seen as

$$\mathbf{W}_{\text{ZF}} = \lim_{\sigma_V \rightarrow 0} \mathbf{W}_{\text{MMSE}}(\sigma_V), \tag{4.11}$$

i.e., in a noiseless transmission, the \mathbf{W}_{MMSE} can be approximated as \mathbf{W}_{ZF} . Therefore, the ZFE can be seen as a special case of the MMSEE in absence of noise.

4.3 Decision Feedback Equalizer

Decision feedback equalizer is a nonlinear equalizer that uses past estimated symbols to make a better decision on the current symbol [39, 77]. The equalization performed by DFE is carried out symbol-by-symbol, as shown in Figure 4.1.

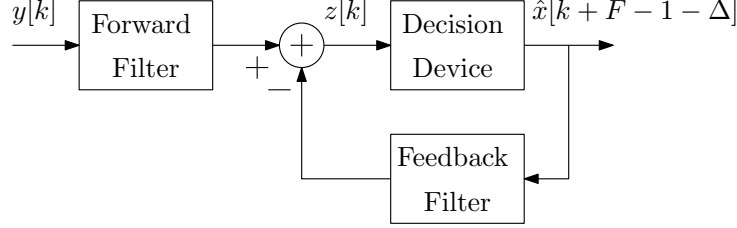


Figure 4.1: Structure for decision feedback equalizer.

The main idea of DFE is to feed back already equalized symbols through a filter to improve the equalization of the current symbol. Any remaining ISI caused by a previous symbol is reconstructed and then subtracted. The DFE is inherently a nonlinear device, but by assuming that all the previous decisions were made correctly, the analysis can be linear [39]. The finite-length DFE consists of a forward filter $\mathbf{w}_f \in \mathbb{C}^{F \times 1}$ given by

$$\mathbf{w}_f = [w[-(F-1)] \ \cdots \ w[-1] \ w[0]]^H, \quad (4.12)$$

and a feedback filter $\mathbf{w}_b \in \mathbb{C}^{B+1 \times 1}$, written as

$$\mathbf{w}_b = [1 \ b[1] \ \cdots \ b[B]]^H. \quad (4.13)$$

4.3.1 DFE Filter Derivation Based on MMSE

To obtain the forward and feedback filters, we need to minimize the MSE at the input of the decision device. The error between the correct symbol $x[k + F - 1 - \Delta]$ and input $z[k]$ at the decision device is given by

$$\begin{aligned} e[k] &= x[k + F - 1 - \Delta] - z[k] \\ &= x[k + F - 1 - \Delta] - \sum_{f \in \mathcal{F}} \mathbf{w}_f^*[-f] y[k + f] + \sum_{b \in \mathcal{B}} \mathbf{w}_b^*[b] x[k + F - 1 - \Delta - b] \\ &= \begin{bmatrix} \mathbf{0}_{1 \times \Delta} & 1 & b^*[1] & \cdots & b^*[B] & \mathbf{0}_{1 \times S} \end{bmatrix} \mathbf{x}[k] - \begin{bmatrix} \mathbf{w}^*[-(F-1)] & \cdots & \mathbf{w}^*[0] \end{bmatrix} \mathbf{y}[k] \end{aligned} \quad (4.14)$$

$$= \tilde{\mathbf{w}}_b^H \mathbf{x}[k] - \mathbf{w}_f^H \mathbf{y}[k], \quad (4.15)$$

where

$$\mathbf{x}[k] = [x[k + F - 1] \ x[k + F] \ \cdots \ x[k - \nu]]^T, \quad (4.16)$$

is the correct symbol vector at instant k , and $\nu = L - 1$,

$$\mathbf{y}[k] = [y[k + F - 1] \ y[k + F] \ \cdots \ y[k]]^T, \quad (4.17)$$

the received symbol vector at instant k .

The constant S in (4.14) is given by

$$S = F - 1 - \Delta, \quad (4.18)$$

where Δ is the decision delay inherent in a causal DFE, satisfying $0 \leq \Delta \leq F + \nu - 2$ [39]. Furthermore, in order to find the forward and backward filter coefficients, we need to compute the MSE of (4.15), written as

$$\begin{aligned} \xi[k] &= \mathbb{E} \{ |e[k]|^2 \} \\ &= \mathbb{E} \{ (\tilde{\mathbf{w}}_b^H \mathbf{x}[k] - \mathbf{w}_f^H \mathbf{y}[k]) (\tilde{\mathbf{w}}_b^H \mathbf{x}[k] - \mathbf{w}_f^H \mathbf{y}[k])^H \} \\ &= \mathbb{E} \{ \tilde{\mathbf{w}}_b^H \mathbf{x}[k] \mathbf{x}[k]^H \tilde{\mathbf{w}}_b - \tilde{\mathbf{w}}_b^H \mathbf{x}[k] \mathbf{y}[k]^H \mathbf{w}_f - \mathbf{w}_f^H \mathbf{y}[k] \mathbf{x}[k]^H \tilde{\mathbf{w}}_b + \tilde{\mathbf{w}}_b^H \mathbf{y}[k] \mathbf{y}[k]^H \tilde{\mathbf{w}}_b \} \\ &= \tilde{\mathbf{w}}_b^H \mathbf{R}_{xx}[k] \tilde{\mathbf{w}}_b - \tilde{\mathbf{w}}_b^H \mathbf{R}_{xy}[k] \mathbf{w}_f - \mathbf{w}_f^H \mathbf{R}_{yx}[k] \tilde{\mathbf{w}}_b + \mathbf{w}_f^H \mathbf{R}_{yy}[k] \mathbf{w}_f, \end{aligned} \quad (4.19)$$

where

$$\mathbf{R}_{xy}[k] = \mathbb{E} \{ \mathbf{x}[k] \mathbf{y}^H[k] \} = \mathbf{R}_{xx}[k] \mathbf{H}^H \quad (4.20)$$

$$\mathbf{R}_{yy}[k] = \mathbb{E} \{ \mathbf{y}[k] \mathbf{y}^H[k] \} = \mathbf{H} \mathbf{R}_{xx}[k] \mathbf{H}^H + \mathbf{R}_{vv}[k], \quad (4.21)$$

By the orthogonality principle, which says that in estimating the realization of a random variable by a linear combination of data samples, the optimal estimator is obtained when the error is orthogonal to each data sample [75]. Therefore, the following relation holds

$$\begin{aligned} \mathbb{E} \{ e[k] \mathbf{y}^H[k] \} &= 0 \Rightarrow \\ \mathbb{E} \{ (\tilde{\mathbf{w}}_b^H \mathbf{x}[k] - \mathbf{w}_f^H \mathbf{y}[k]) \mathbf{y}^H[k] \} &= 0 \\ \mathbb{E} \{ \tilde{\mathbf{w}}_b^H \mathbf{x}[k] \mathbf{y}^H[k] - \mathbf{w}_f^H \mathbf{y}[k] \mathbf{y}^H[k] \} &= 0 \\ \tilde{\mathbf{w}}_b^H \mathbf{R}_{xy}[k] - \mathbf{w}_f^H \mathbf{R}_{yy}[k] &= 0 \\ \tilde{\mathbf{w}}_b^H \mathbf{R}_{xy}[k] &= \mathbf{w}_f^H \mathbf{R}_{yy}[k]. \end{aligned} \quad (4.22)$$

Then, by using (4.22), (4.19) can be rewritten as

$$\begin{aligned}\xi[k] &= \tilde{\mathbf{w}}_b^H \mathbf{R}_{xx}[k] \tilde{\mathbf{w}}_b - \mathbf{w}_f^H \mathbf{R}_{yy}[k] \mathbf{w}_f - \mathbf{w}_f^H \mathbf{R}_{yx} \tilde{\mathbf{w}}_b + \mathbf{w}_f^H \mathbf{R}_{yy}[k] \mathbf{w}_f \\ &= \tilde{\mathbf{w}}_b^H \mathbf{R}_{xx}[k] \tilde{\mathbf{w}}_b - \mathbf{w}_f^H \mathbf{R}_{yx} \tilde{\mathbf{w}}_b,\end{aligned}\quad (4.23)$$

yielding,

$$\mathbf{w}_f^H = \tilde{\mathbf{w}}_b^H \mathbf{R}_{xy}[k] \mathbf{R}_{yy}[k]^{-1}. \quad (4.24)$$

Thus, (4.23) is given by

$$\begin{aligned}\xi[k] &= \tilde{\mathbf{w}}_b^H \mathbf{R}_{xx}[k] \tilde{\mathbf{w}}_b - \tilde{\mathbf{w}}_b^H \mathbf{R}_{xy}[k] \mathbf{R}_{yy}[k]^{-1} \mathbf{R}_{yx} \tilde{\mathbf{w}}_b \\ &= \tilde{\mathbf{w}}_b^H (\mathbf{R}_{xx}[k] - \mathbf{R}_{xy}[k] \mathbf{R}_{yy}[k]^{-1} \mathbf{R}_{yx}) \tilde{\mathbf{w}}_b\end{aligned}\quad (4.25)$$

with $\mathbf{R}_{yy}[k] = \mathbf{H} \mathbf{R}_{xx}[k] \mathbf{H}^H + \mathbf{R}_{vv}[k]$, $\mathbf{R}_{xy}[k] = \mathbf{R}_{xx}[k] \mathbf{H}^H$ and $\mathbf{R}_{yx} = \mathbf{H} \mathbf{R}_{xx}[k]$,

$$\xi[k] = \tilde{\mathbf{w}}_b^H (\mathbf{R}_{xx}[k] - \mathbf{R}_{xx}[k] \mathbf{H}^H (\mathbf{H} \mathbf{R}_{xx}[k] \mathbf{H}^H + \mathbf{R}_{vv}[k])^{-1} \mathbf{H} \mathbf{R}_{xx}[k]) \tilde{\mathbf{w}}_b. \quad (4.26)$$

From the Woodbury¹ matrix identity [78],

$$\mathbf{R}_{xx}[k] - \mathbf{R}_{xx}[k] \mathbf{H}^H (\mathbf{H} \mathbf{R}_{xx}[k] \mathbf{H}^H + \mathbf{R}_{vv}[k])^{-1} \mathbf{H} \mathbf{R}_{xx}[k] = (\mathbf{R}_{xx}[k]^{-1} + \mathbf{H}^H \mathbf{R}_{vv}[k]^{-1} \mathbf{H})^{-1}, \quad (4.27)$$

then, (4.26) becomes

$$\xi[k] = \tilde{\mathbf{w}}_b^H (\mathbf{R}_{xx}[k]^{-1} + \mathbf{H}^H \mathbf{R}_{vv}[k]^{-1} \mathbf{H})^{-1} \tilde{\mathbf{w}}_b \quad (4.28)$$

By defining

$$\mathbf{R}_\Delta = \mathbf{Q} (\mathbf{R}_{xx}[k]^{-1} + \mathbf{H}^H \mathbf{R}_{vv}[k]^{-1} \mathbf{H})^{-1} \mathbf{Q}^T, \quad (4.29)$$

where $\mathbf{Q} = [\mathbf{0}_{(B+1) \times \Delta} \quad \mathbf{I}_{(B+1)} \quad \mathbf{0}_{(B+1) \times S}]$, (4.29) is given by

$$\xi[k] = \mathbf{w}_b^H \mathbf{R}_\Delta \mathbf{w}_b. \quad (4.30)$$

Equation (4.30) is a quadratic form that is minimized by choosing the feedback filter as

$$\mathbf{w}_b = \frac{\mathbf{R}_\Delta^{-1} \mathbf{e}_0}{\mathbf{e}_0^T \mathbf{R}_\Delta^{-1} \mathbf{e}_0}, \quad (4.31)$$

where \mathbf{e}_0 is the first column of \mathbf{I}_B . The forward filter can be computed as

$$\mathbf{w}_f^H = \tilde{\mathbf{w}}_b^H \mathbf{R}_{xy}[k] \mathbf{R}_{yy}[k]^{-1}, \quad (4.32)$$

¹Woodbury's identity $(\mathbf{A} + \mathbf{UCV})^{-1} = \mathbf{A}^{-1} - \mathbf{A}^{-1} \mathbf{U} (\mathbf{C}^{-1} + \mathbf{VA}^{-1} \mathbf{U})^{-1} \mathbf{VA}^{-1}$

4.3.2 Enhancing the DFE Computational Performance

Extending the DFE analysis, some assumptions are going to be considered to enhance the DFE computational performance. The first assumption is that the number of taps of the feedback filter is equal to the channel memory, i.e., $B = \nu$ [39]. Under this assumption, the Cholesky decomposition is applied on (4.27) [79]. The decomposition can be written as

$$\mathbf{L}\mathbf{D}\mathbf{L}^H = \mathbf{R}_{xx}[k]^{-1} + \mathbf{H}^H\mathbf{R}_{vv}[k]^{-1}\mathbf{H} \quad (4.33)$$

where $\mathbf{L} \in \mathbb{C}^{F+\nu \times F+\nu}$ is a lower triangular matrix and $\mathbf{D} \in \mathbb{C}^{F+\nu \times F+\nu}$ is the diagonal matrix $\mathbf{D} = \text{Diag}\{\mathbf{d}\}$, and

$$\mathbf{d} = \begin{bmatrix} d[0] & d[1] & \dots & d[F - \nu - 1] \end{bmatrix}^T, \quad (4.34)$$

are the matrices from the Cholesky decomposition of (4.27). From (4.28) and (4.33), the MSE becomes

$$\xi[k] = \tilde{\mathbf{w}}_b^H \mathbf{L}^{-H} \mathbf{D}^{-1} \mathbf{L}^{-1} \tilde{\mathbf{w}}_b. \quad (4.35)$$

Equation (4.35) is minimized by choosing Δ from (4.18) such as $\tilde{\mathbf{w}}_b$ matches the column of \mathbf{L} whose index is equal to the index of

$$d_{\Delta_{\text{opt}}} = \max\{\mathbf{d}\}. \quad (4.36)$$

This index is equal to the optimum delay Δ_{opt} . Hence,

$$\tilde{\mathbf{w}}_{b,\text{opt}} = \mathbf{L}\mathbf{e}_{(\Delta_{\text{opt}}+1)}, \quad (4.37)$$

where \mathbf{e}_j is the j th column of $\mathbf{I}_{F+\nu}$. Therefore, the minimum MSE is given by

$$\xi_{\min} = d_{\Delta_{\text{opt}}}^{-1}. \quad (4.38)$$

The optimum feedforward filter $\mathbf{w}_{f,\text{opt}}^H$ is computed as

$$\begin{aligned} \mathbf{w}_{f,\text{opt}}^H &= \tilde{\mathbf{w}}_{b,\text{opt}}^H \mathbf{R}_{xy}[k] \mathbf{R}_{yy}[k]^{-1} \\ &= \tilde{\mathbf{w}}_{b,\text{opt}}^H \mathbf{R}_{xx}[k] \mathbf{H}^H (\mathbf{H} \mathbf{R}_{xx}[k] \mathbf{H}^H + \mathbf{R}_{vv}[k])^{-1} \\ &= \tilde{\mathbf{w}}_{b,\text{opt}}^H \mathbf{R}_{xx}[k] \mathbf{H}^H \left(\mathbf{R}_{vv}[k]^{-1} - \mathbf{R}_{vv}[k]^{-1} \mathbf{H} (\mathbf{H}^H \mathbf{R}_{vv}[k]^{-1} \mathbf{H} + \mathbf{R}_{xx}[k]^{-1})^{-1} \mathbf{H}^H \mathbf{R}_{vv}[k]^{-1} \right) \\ &= \tilde{\mathbf{w}}_{b,\text{opt}}^H \mathbf{R}_{xx}[k] \left(\mathbf{I}_{N+L} - \mathbf{H}^H \mathbf{R}_{vv}[k]^{-1} \mathbf{H} (\mathbf{H}^H \mathbf{R}_{vv}[k]^{-1} \mathbf{H} + \mathbf{R}_{xx}[k]^{-1})^{-1} \mathbf{H}^H \mathbf{R}_{vv}[k]^{-1} \right) \\ &= \tilde{\mathbf{w}}_{b,\text{opt}}^H (\mathbf{R}_{xx}[k] + \mathbf{H}^H \mathbf{R}_{vv}[k]^{-1} \mathbf{H}) \mathbf{H}^H \mathbf{R}_{vv}[k]^{-1} \\ &= d_{\Delta_{\text{opt}}}^{-1} \mathbf{e}_{(\Delta_{\text{opt}}+1)}^H \mathbf{L}^{-1} \mathbf{H}^H \mathbf{R}_{vv}[k]^{-1}. \end{aligned} \quad (4.39)$$

In [39] is shown that the optimum Δ is given by $\Delta_{\text{opt}} = F - 1$, which is verified through extensive computer simulations that this assumption holds for most practical channel and noise scenarios. This assumption on Δ yields $S = 0$. Moreover, the length of the forward and feedback filters are related to the length of the channel. Thus, it is shown in [80] that the DFE computational performance is enhanced with $F = 2\nu$ and $B = \nu$.

4.4 Turbo Equalizer

Equalization and decoding are typically analyzed separately, as the equalizers previously presented in Section 4.1 with ZFE and in Section 4.2 with MMSEE. The primary reason for manipulating them separated from each other is the computational complexity burden in doing it together [37]. A receiver algorithm where the equalizer is aware of the underlying code is often nominated joint equalization and decoding. Many iterative receiver algorithms repeat the joint equalization and decoding tasks on the same assemblage of data, where feedback information from the decoder is combined into the equalization process. This method is the basis of turbo equalization and is based on decoding methods for turbo codes [43].

The TEQ were first proposed in [81] and since then has been adapted to various communication tasks, ranging from detection and decoding of *trellis coded modulation* (TCM) [82, 83], *code division multiple access* (CDMA) [84] and optical fiber communications [85]. One application area in which turbo equalization has been extensively employed is UWA communications, achieving great performances in terms of BER [86, 87, 88, 89]. This is the reason behind choosing TEQ for this project.

4.4.1 Separate Equalization *versus* Joint Equalization

A standard approach to separate equalization and decoding is employed as the structure represented in Figure 3.1. The receiver communicates estimates $\hat{x}[k]$, $\hat{c}[k]$ and $\hat{b}[k]$, from the same alphabet as $x[k]$, $c[k]$ and $b[k]$, respectively, from the equalizer to the decoder, trading between them what is called hard information. Two traditional families of algorithms for the sub-problem of equalization are those based

on trellis methods [90] and those using linear filters. Linear filter-based approaches perform linear operations on the received symbols, which can be represented with matrix operations on the sequence directly. Examples are the ZFE and MMSEE presented in this chapter. However, the equalizer can often provide more information to the decoder than the hard information $\hat{x}[k]$ at the cost of additional storage, processing, and communication, such as probabilities that $x[k]$ takes on a particular symbol from alphabet employed in the transmission. The principle of using probabilities (soft information) rather than hard-decisions is often referred to as soft processing or soft decoding.

The procedure of passing soft information in joint equalization and decoding was first proposed by [43] in the context of decoding turbo codes. Since then, it has been extended to various concatenated communication systems such as coded data transmission over ISI channels, where it is called *turbo equalization*. The exact implementation of joint equalization and decoding is intractable for a general code and interleaver because of computational complexity reasons. Hence a feasible sub-optimal alternative is typically wanted [37].

The method employed in this project consists of linear processing of the received signal incorporated on the turbo equalization method. The parameters of these equalizers can be optimized using a variety of optimization algorithms, such as ZF or MMSE estimations. Methods for minimizing the BER or the *symbol error rate* (SER) are highly nonlinear [37]. These nonlinear methods are based on *maximum likelihood* (ML) estimation, which turns into MAP estimation in the presence of *a priori* knowledge regarding the transmitted data. Effective algorithms exist for MAP/ML sequence estimation, such as the Viterbi algorithm [62, 91], for MAP/ML symbol estimation, such as the BCJR algorithm [90]. However, the complexity of such techniques often remains significantly higher than that for linear methods. This high complexity is true in particular for channels with large delay spread, which is the case for UWA channels. The alternative employed in this project is the one that uses a SISO equalization based on linear MMSE estimation.

4.4.2 The Turbo Principle

The idea displayed in Figure 4.2 is an iterative receiver method, which summarizes how TEQ works. The receiver recomputes the soft information (Equalizer to Decoder) and (Decoder to Equalizer) by iterating equalization and decoding tasks multiple times, passing soft information between them.

Consider the following approach. The receiver computes the soft information $\mathbf{s}(C[k])$ and $\mathbf{s}(B[k])$ followed by decoding, where $C[k]$ and $B[k]$ are the Demapper and Deinterleaver outputs, respectively, as in Figure 4.2. At this stage, the decoder may compute a new version of the soft information $\mathbf{s}(B[k])$, given by

$$\mathbf{s}'(B[k]) = \Pr \{B[k] \mid \mathbf{s}(B[1]), \mathbf{s}(B[2]), \dots, \mathbf{s}(B[N])\}. \quad (4.40)$$

The reliability of $\mathbf{s}'(B[k])$ compared to $\mathbf{s}(B[k])$ generally improves because of the redundancy introduced during FEC encoding, i.e., the values in $\mathbf{s}'(B[k])$ are closer to 0 and 1 than $\mathbf{s}(B[k])$. After interleaving $\mathbf{s}'(B[k])$ and $\mathbf{s}'(C[k])$, it makes sense to use the new soft information $\mathbf{s}'(C[k])$ to guide the equalizer with new symbol probabilities $\mathbf{s}'(X[k])$. Assuming a *binary phase-shift keying* (BPSK) modulation, the mapping is done as $\mathbf{s}'(X[k] = +1) = \mathbf{s}'(C[k] = 0)$ and $\mathbf{s}'(X[k] = -1) = \mathbf{s}'(C[k] = 1)$. Having the soft information $\mathbf{s}'(X[k])$, it is possible to repeat the equalization step, yielding updated soft information $\mathbf{s}(X[k])$. The whole process amounts to joint equalization and decoding, since the equalizer incorporates knowledge about the underlying code. For reasons discussed in [37], the BER can be improved tremendously when the following information is fed back from the decoder to equalizer

$$\mathbf{s}'_{\text{ext}}(B[k]) = \Pr \{B[k] \mid \mathbf{s}(B[1]), \mathbf{s}(B[2]), \dots, \mathbf{s}(B[k-1]), \mathbf{s}(B[k+1]), \dots, \mathbf{s}(B[K])\}. \quad (4.41)$$

This quantity is the *extrinsic soft information* about $B[k]$ contained in $\mathbf{s}(B[1]), \mathbf{s}(B[2]), \dots, \mathbf{s}(B[K])$ except $\mathbf{s}(B[k])$. Similarly, the equalizer should communicate extrinsic soft information $\mathbf{s}_{\text{ext}}(C[k])$ to the decoder computed using the observation \mathbf{y} and all $\mathbf{s}'_{\text{ext}}(C[1]), \mathbf{s}'_{\text{ext}}(C[2]), \dots, \mathbf{s}'_{\text{ext}}(C[K])$ except $\mathbf{s}'_{\text{ext}}(C[k])$. This approach to passing extrinsic soft information in communication systems is called *turbo equalization*. Since the code bits $b[k]$ are from a binary alphabet, $\mathbf{s}(B[k] = 0)$ and $\mathbf{s}(B[k] = 1)$ are

replaced by the *log-likelihood ratio* (LLR)

$$\lambda(B[k]) = \ln \frac{s(B[k] = 0)}{s(B[k] = 1)}. \quad (4.42)$$

The analogous extrinsic LLRs $\lambda_{\text{ext}}(B[k])$ and $\lambda_{\text{ext}}(C[k])$ are used in further development.

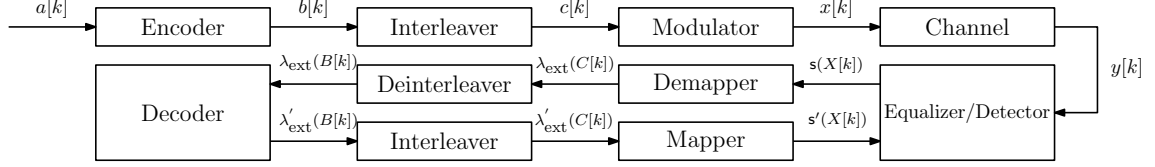


Figure 4.2: Structure of Turbo Equalizer for a baseband communication system.

4.4.3 Derivating the Turbo Equalizer Algorithm

This section shows how to compute the estimation $\hat{x}[k]$ and the LLRs involved in a turbo iteration. At the end, Table 1 summarizes what was presented.

Figure 4.3 shows a SISO equalizer employing the linear MMSE estimation. This is done by mapping the LLRs $\lambda'_{\text{ext}}(C[k])$ to probabilities $s'(X[k])$ followed by mapping them to new statistics $\mu_X[k] = \mathbb{E}\{X[k]\}$ and $\sigma_X^2[k] = \text{Var}\{X[k]\}$. The mean, $\mu_X[k]$ can be written as

$$\begin{aligned} \mu_X[k] &= \sum_{x \in \mathcal{C}} x s'(X[k] = x) \\ &= s'(X[k] = +1) - s'(X[k] = -1) \\ &= s'(C[k] = 0) - s'(C[k] = 1) \\ &= \frac{1}{1 + e^{-\lambda'_{\text{ext}}(C[k])}} - \frac{e^{-\lambda'_{\text{ext}}(C[k])}}{1 + e^{-\lambda'_{\text{ext}}(C[k])}} \\ &= \tanh\left(\frac{e^{\lambda'_{\text{ext}}(C[k])}}{2}\right), \end{aligned} \quad (4.43)$$

and the variance $\sigma_X^2[k]$ is written as follows

$$\begin{aligned} \sigma_X^2[k] &= \sum_{x \in \mathcal{C}} |x - \mathbb{E}\{X[k]\}|^2 s'(X[k] = x) \\ &= 1 - |\mu_X[k]|^2. \end{aligned} \quad (4.44)$$

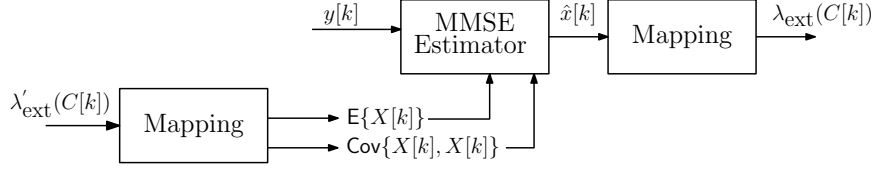


Figure 4.3: A SISO equalizer based on linear MMSE estimation.

A second step is to map the symbol estimates $\hat{x}[k]$ produced from the linear MMSE estimator to the extrinsic LLRs $\lambda_{\text{ext}}(C[k])$. The following rule can be used to compute $\lambda_{\text{ext}}(C[k])$

$$\begin{aligned} \lambda_{\text{ext}}(C[k]) &= \ln \frac{s_{\text{ext}}(C[k] = 0)}{s_{\text{ext}}(C[k] = 1)} \\ &= \ln \frac{s(X[k] = +1)}{s(X[k] = -1)} \bigg|_{\text{without using } \lambda'_{\text{ext}}(C[k])}, \end{aligned} \quad (4.45)$$

where $s(X[k] = x)$ is the value of the *probability density function* (PDF) $f_E(e[k])$ evaluated at $e[k] = \hat{x}[k] - x$. The estimation error $e[k]$ is a realization of the RV $E[k] \sim \mathcal{N}(\mathbf{E}\{E[k]\}, \mathbf{Var}\{E[k]\})$. The extrinsic LLR $\lambda_{\text{ext}}(C[k])$ should not depend on $\lambda'_{\text{ext}}(C[k])$ and, consequently, neither should the estimate $\hat{x}[k]$ depend on $\lambda'_{\text{ext}}(C[k])$, which affects the derivation of the estimation algorithm.

The linear MMSE estimator considered here processes a length- W window of observations

$$\mathbf{y}[k] = [y[k - W_2] \ y[k - W_2 + 1] \ \dots \ y[k + W_1]]^T, \quad (4.46)$$

where $W = W_1 + W_2 + 1$, rather than the complete sequence \mathbf{y} to compute the estimate $\hat{x}[k]$. This approach minimizes the computational complexity, reducing the amount of data to be processed in each iteration [37]. From the ISI model in (3.25), the estimate $\hat{x}[k]$ of $x[k]$ that minimizes the $\xi[k]$ is given by

$$\begin{aligned} \hat{x}[k] &= \mathbf{E}\{X[k]\} + \mathbf{Cov}\{X[k], \mathbf{y}[k]\} \mathbf{Cov}\{\mathbf{y}[k], \mathbf{y}[k]\}^{-1} (\mathbf{y}[k] - \mathbf{E}\{\mathbf{y}[k]\}) \\ &= \mu_X[k] + \sigma_X^2[k] \mathbf{h}^T[k] \mathbf{\Sigma}^{-1}[k] (\mathbf{y}[k] - \mathbf{H}[k] \boldsymbol{\mu}_X[k]), \end{aligned} \quad (4.47)$$

where

$$\mathbf{\Sigma}[k] = \sigma_V^2 \mathbf{I}_W + \mathbf{H}[k] \mathbf{V}[k] \mathbf{H}^T[k], \quad (4.48)$$

and $\mathbf{H}[k] \in \mathbb{C}^{W \times (W+\nu)}$, is the submatrix $\mathbf{H}[k - W_2 : k + W_1, k - W_2 - \nu : k + W_1]$ of the system matrix \mathbf{H} . The following $\mathbf{H}[k]$ is given for $k = W_2 + 1$, and the same structure is used for the remaining time indices [37]

$$\mathbf{H}[k] = \begin{bmatrix} h_\nu & h_{\nu-1} & \dots & 0 & 0 & \dots & 0 \\ 0 & h_\nu & h_{\nu-1} & \dots & h_1 & 0 & \dots & 0 \\ & & & \ddots & & & & \\ 0 & & \dots & 0 & h_\nu & h_{\nu-1} & \dots & h_1 \end{bmatrix}, \quad (4.49)$$

and

$$\boldsymbol{\mu}_X[k] = [\mu_X[k - \nu - W_2] \ \mu_X[k - \nu - W_2 + 1] \ \dots \ \mu_X[k + W_1]]^T, \quad (4.50)$$

$$\mathbf{V}[k] = \text{Diag} \left\{ [\sigma_X^2[k - \nu - W_2] \ \sigma_X^2[k - \nu - W_2 + 1] \ \dots \ \sigma_X^2[k + W_1]]^T \right\}, \quad (4.51)$$

$$\mathbf{h}[k] = \mathbf{h}_{W_2+\nu}[k]. \quad (4.52)$$

The estimate $\hat{x}[k]$ calculated in (4.47) depends on $\lambda'_{\text{ext}}(C[k])$ via $\mu_X[k]$ and $\sigma_X^2[k]$. In order that $\hat{x}[k]$ be independent from $\lambda'_{\text{ext}}(C[k])$, this particular LLR is set to 0 while computing $\hat{x}[k]$. This choice corresponds to an *independent uniformly distributed* (IUD) assumption made on the particular symbol $x[k]$. It follows that $\mu_X[k]$ and $\sigma_X^2[k]$ should be replaced by 0 and 1, respectively, while computing the estimated $\hat{x}[k]$, which changes (4.47) to

$$\hat{x}[k] = \mathbf{h}^T[k] \left(\underbrace{\boldsymbol{\Sigma}[k] + (1 - \sigma_X^2[k]) \mathbf{h}[k] \mathbf{h}^T[k]}_{\mathbf{A}[k]} \right)^{-1} (\mathbf{y}[k] - \mathbf{H}[k] \boldsymbol{\mu}_X[k] + \mu_X[k] \mathbf{h}[k]) \quad (4.53)$$

Using the Sherman-Morrison formula², a special case of the Woodbury's identity, the expression $\mathbf{h}^T[k] \mathbf{A}^{-1}[k]$ can be simplified as follows:

$$\begin{aligned} \mathbf{h}^T[k] \mathbf{A}^{-1}[k] &= \mathbf{h}^T[k] \boldsymbol{\Sigma}^{-1}[k] - \frac{\mathbf{h}^T[k] \boldsymbol{\Sigma}^{-1}[k] \mathbf{h}[k] \mathbf{h}^T[k] \boldsymbol{\Sigma}^{-1}[k]}{(1 - \sigma_X^2[k])^{-1} + \mathbf{h}^T[k] \boldsymbol{\Sigma}^{-1}[k] \mathbf{h}[k]} \\ &= \mathbf{f}^T[k] - \frac{\mathbf{f}^T[k] \mathbf{h}[k] \mathbf{f}^T[k]}{(1 - \sigma_X^2[k])^{-1} + \mathbf{f}^T[k] \mathbf{h}[k]} \\ &= \frac{\mathbf{f}^T[k]}{1 + (1 - \sigma_X^2[k]) \mathbf{f}^T[k] \mathbf{h}[k]}, \end{aligned} \quad (4.54)$$

²Sherman-Morrison formula $(\mathbf{A} + \mathbf{u} \mathbf{v}^T)^{-1} = \mathbf{A}^{-1} - \frac{\mathbf{A}^{-1} \mathbf{u} \mathbf{v}^T \mathbf{A}^{-1}}{1 + \mathbf{v}^T \mathbf{A}^{-1} \mathbf{u}}$

where

$$\begin{aligned}\mathbf{f}[k] &= \mathbf{\Sigma}^{-1}[k]\mathbf{h}[k] \\ &= (\sigma_V^2 \mathbf{I}_W + \mathbf{H}[k]\mathbf{V}[k]\mathbf{H}^T[k])^{-1} \mathbf{h}[k].\end{aligned}\quad (4.55)$$

The estimate $\hat{x}[k]$ is now given by

$$\hat{x}[k] = \frac{\mathbf{f}^T[k] (\mathbf{y}[k] - \mathbf{H}[k]\boldsymbol{\mu}_x[k]) + \mu_X[k]s[k]}{1 + (1 - \sigma_X^2[k])s[k]}, \quad (4.56)$$

where

$$s[k] = \mathbf{f}^T[k]\mathbf{h}[k]. \quad (4.57)$$

To calculate the extrinsic LLRs $\lambda_{\text{ext}}(C[k])$, we have that the mean and the variance of the estimation error $e[k] = \hat{x}[k] - x[k]$ are given by $\mathbf{E}\{E[k]\} = 0$ and under the constraint that $\sigma_X^2[k]$ is replaced by 1 yields

$$\begin{aligned}\text{Var}\{E[k]\} &= 1 - \mathbf{h}[k]^T (\mathbf{\Sigma}[k] + (1 - \sigma_X^2[k]) \mathbf{h}[k]\mathbf{h}[k]^T)^{-1} \mathbf{h}[k] \\ &= 1 - \frac{\mathbf{f}[k]^T \mathbf{h}[k]}{1 + (1 - \sigma_X^2[k]) \mathbf{f}[k]^T \mathbf{h}[k]} \\ &= 1 - \frac{s[k]}{1 + (1 - \sigma_X^2[k])s[k]}\end{aligned}\quad (4.58)$$

where again Sherman-Morrison formula was applied. Under the Gaussian assumption, the extrinsic LLRs $\lambda_{\text{ext}}(C[k])$ for BPSK modulation are given by

$$\begin{aligned}\lambda_{\text{ext}}(C[k]) &= \ln \frac{e^{-(\hat{x}[k] - (+1))^2 / 2\text{Var}\{E[k]\}}}{e^{-(\hat{x}[k] - (-1))^2 / 2\text{Var}\{E[k]\}}} \\ &= \frac{2\hat{x}[k]}{1 - \frac{s[k]}{(1 + (1 - \sigma_X^2[k])s[k])}} \\ &= \frac{2(\mathbf{f}^T[k] (\mathbf{y}[k] - \mathbf{H}[k]\boldsymbol{\mu}_X[k]) + \mu_X[k]s[k])}{1 - \sigma_X^2[k]s[k]}\end{aligned}\quad (4.59)$$

The Algorithm 1 brings the algorithm for the TEQ using BPSK-modulated bits that was derived in this chapter.

Algorithm 1 SISO Equalization Algorithm Based on Linear MMSE Estimation of BPSK-modulated Signals

INPUT

extrinsic LLRs $\lambda'_{\text{ext}}(C[k])$ for $k \in \mathcal{K} = [1, \dots, K]$

INITIALIZATION

compute $\mu_X[k] = \tanh(\lambda'_{\text{ext}}(C[k])/2)$ and $\sigma_X^2[k] = 1 - |\mu_X[k]|^2$

LINEAR MMSE ESTIMATION

FOR $k = 1$ **TO** K **DO**

$$\mathbf{f}[k] = (\sigma_V^2 \mathbf{I}_W + \mathbf{H}[k] \mathbf{V}[k] \mathbf{H}^T[k])^{-1} \mathbf{h}[k]$$

$$s[k] = \mathbf{f}^T[k] \mathbf{h}[k]$$

$$\lambda_{\text{ext}}(C[k]) = \frac{2(\mathbf{f}^T[k](\mathbf{y}[k] - \mathbf{H}[k] \boldsymbol{\mu}_X[k]) + \mu_X[k] s[k])}{1 - \sigma_X^2[k] s[k]}$$

END

4.4.4 On the Effect of Multiple Turbo Iterations

In order to properly finish this section about the TEQ, an example is given on the effect of multiple turbo iterations in a BPSK-modulated transmitted signal constellation. In Figure 4.4 we have the received signal, before any equalization, the SNR is 10 dB. The SNR of 10 dB was chosen for this example to match the SNR estimated in practical experiment explored in [57].

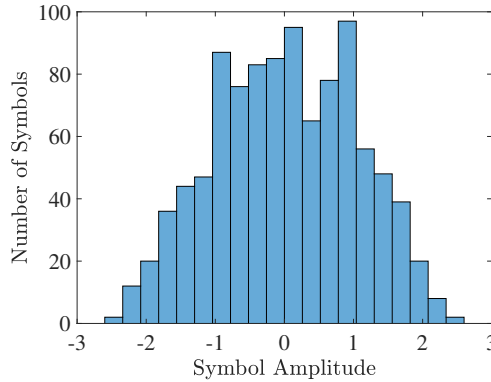
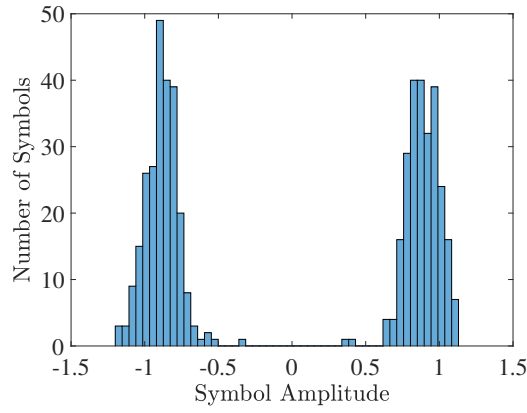


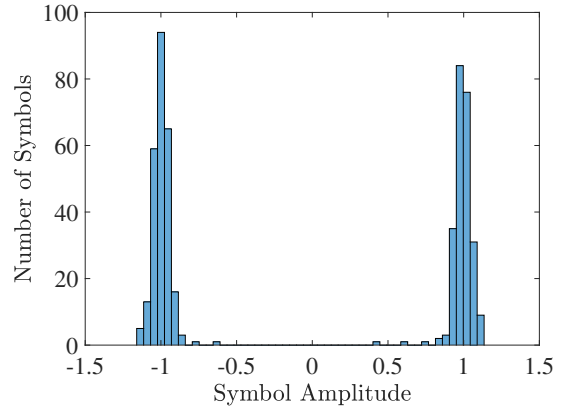
Figure 4.4: Constellation of received signal, SNR = 10 dB.

Figure 4.5 shows how the constellation of the received signal behaves on multiple turbo iterations. From the second iteration, Figure 4.5a, to the eighth iteration, Figure 4.5d, it is patent the enhancement on the equalization results. After the eighth iteration the equalized symbols are entirely on the immediate vicinity of -1 and 1 .

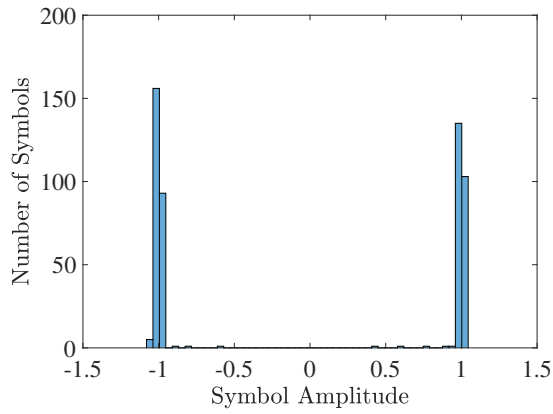
In conclusion, the example helps visualize how the turbo iterations effectively increase the BER on the receiver.



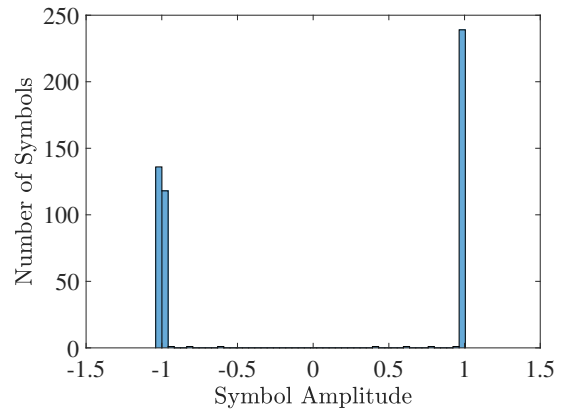
(a) Symbol histogram after 2 turbo iterations.



(b) Symbol histogram after 3 turbo iterations.



(c) Symbol histogram after 5 turbo iterations.



(d) Symbol histogram after 8 turbo iterations.

Figure 4.5: Example on the effect of multiple turbo equalization iterations.

Chapter 5

Simulations & Results

This chapter presents simulations using characteristics of UWA channels and employing the equalizer presented on Chapter 4. Different transmission scenarios are explored in order to compare the performances of the equalizers. Results are presented as graphics with BER on the ordinate and ascending SNR levels on the abscissa.

5.1 Simulation Scenarios

The different simulation scenarios were generated using a framework to produce CIRs of UWA channels using a stochastic-based channel simulator, presented in [66], and a model-based CIR replay tool, e.g., TRACEO.

Once the model-based CIR replay tool is fed with information regarding transmission-site bathymetry and sound speed profile, then it outputs the necessary data to run the stochastic-based channel simulator. Table 5.1 displays the information acquired processing the data from the model-based CIR replay tool, which for this project the TRACEO [92] was employed. Using Table 5.1 it is possible to reproduce the CIRs employed in the simulations on this work.

It is important to note that the purpose of using the proposed framework to generate CIRs for this project is to emulate more challenging practical channels conditions rather than having carefully crafted CIRs that would benefit the simulation results.

Table 5.1: Channel Characteristics for Simulation.

	Distance (km)				
Parameter	0.5	1.0	2.0	5.0	10.0
Number of Paths	30	17	14	12	9
Delay Spread (ms)	47.2	49.1	48.1	51.4	45.1
Delay Mean (ms)	1.4	3.1	3.7	4.8	6.0
Attenuation (dB)	51.3	60.2	68.8	90.1	124.6

The bathymetric profile used to run the model-based CIR replay tool ends at 10 km. Hence this was a limitation imposed by the available data on the maximum transmission distance. The bathymetry information was gathered in Arraial do Cabo, ($22^{\circ}58'38.2''\text{S}$, $42^{\circ}01'10.4''\text{W}$), illustrated in Figure 5.1, and provided along with sound speed profile data collected in the same area by the IEAPM.

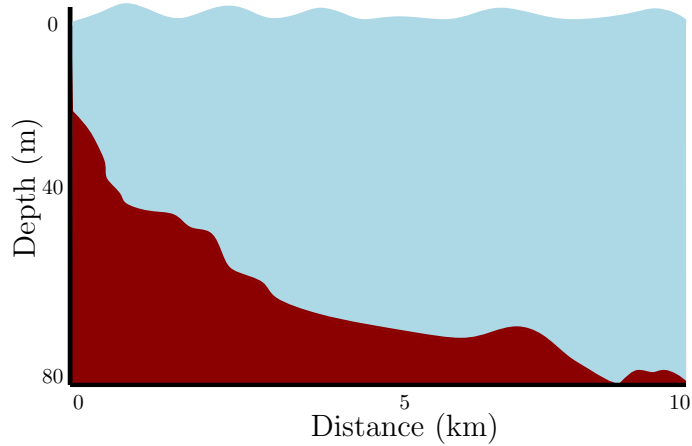


Figure 5.1: Illustration of the 10 km bathymetric profile provided by the IEAPM, collected in Arraio do Cabo.

5.1.1 On the Relation Between the Channel Characteristics and Channel Examples

Figures 5.2, 5.3 and 5.4 display examples of CIRs generated using the stochastic-based channel simulator [66]. The CIRs were produced using information given by Table 5.1. The first information on the table, Number of Paths, is straightforward to see how it affects the CIR. Each example has the exactly number of taps given by the Number of Paths row.

To understand each row of Table 5.1, it is essential to know that the stochastic-based channel simulator employed the discrete-time equivalent of equation (3.17), generating LTI channels. And that this work does not consider Doppler effect on the transmission to focus on the equalizer performances. The parameters left to set are the path gains and the path delays. The former uses a Rayleigh distribution where each path gain is computed using the Attenuation parameter (last row of Table 5.1) as the attenuation that occurs during Delay Spread (second row of Table 5.1). The path delays are computed using an Exponential PDF where Delay Mean (third row of Table 5.1) is the PDF mean value.

Furthermore, this gives a glance on how the following CIRs were computed in order to reproduce an ensemble with the same statistical characteristics. Figure 5.2 displays examples on CIRs for 500 m and 1 km channels. These are quite challenging channels because they have a great number of paths.

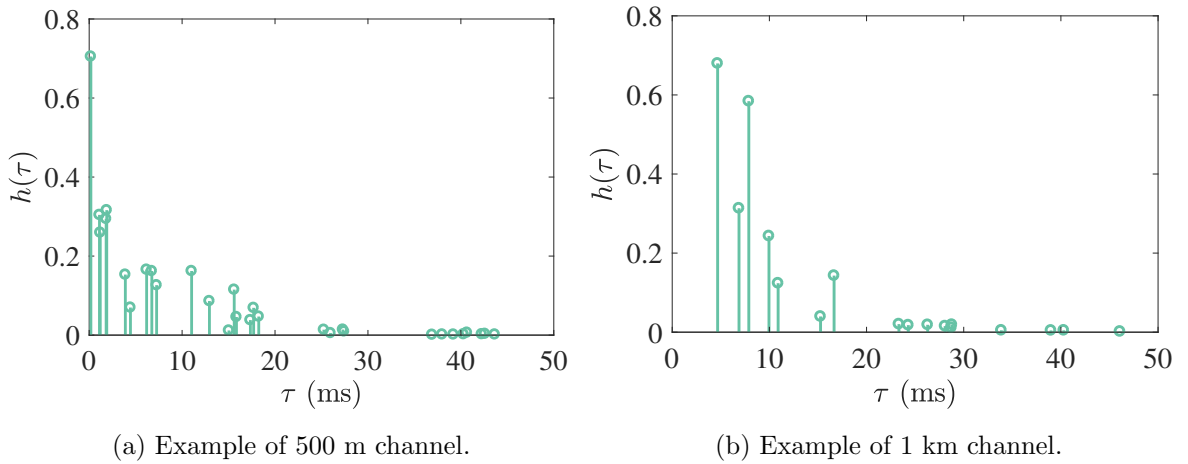


Figure 5.2: Example of channels for 500 m and 1 km to illustrate the CIR.

Moreover, we have examples of channels for 2 km and 5 km in Figure 5.3, and 10 km in Figure 5.4. A total number of 10,000 CIRs for each distance were produced for simulations. This is made possible by the stochastic-based channel simulator [66], enabling us to make Monte Carlo simulations to evaluate the equalizer performances.

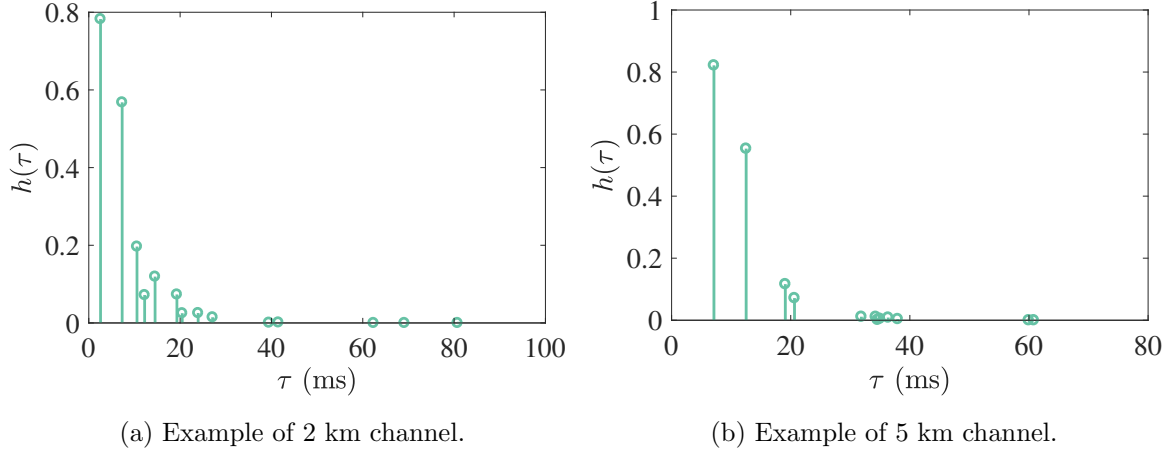


Figure 5.3: Example of channels for 2 km and 5 km.

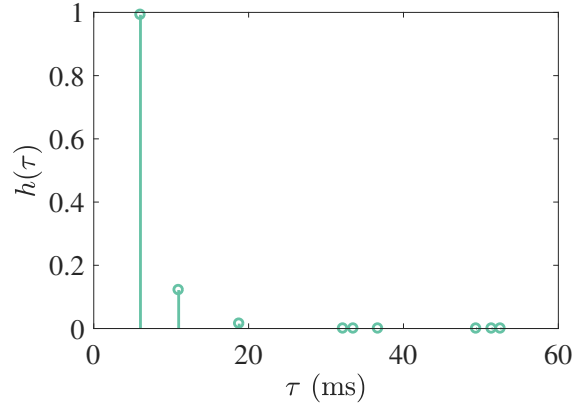


Figure 5.4: Example of 10 km channel.

5.2 Simulation Results

Simulations using the channel previously presented and employing the ZFE, MM-SEE, DFE, and TEQ were carried out for different scenarios.

5.2.1 Communication System & Turbo Equalizer Parameters Used on Simulations

It is necessary to inform a few parameters used on the communication system for the simulations to make possible reproducing them. Bear in mind that the equalizer performances on the UWA channels were the primordial analysis to be made. Hence the communication system might not employ the most efficient FEC, and knowledge of the best least-squares estimation of the channel is used. Some parameters were

chosen to match already used settings on practical experiments conducted by our group [57]. Other parameters were set to approximate the ones described in [37], to make possible some comparison on the TEQ BER performance.

For each Monte Carlo iteration there were 500 generated bits. During each Monte Carlo, the SNR varied from 0 through 18 dB, with a 2 dB step. BPSK modulation scheme and an encoder using a convolutional code given by the generator polynomials $g_0(D) = 1 + D^2$ and $g_1(D) = 1 + D + D^2$ were employed. The given convolutional code was adopted based in [37]. Also based in the same paper, a maximum number of 8 turbo iterations were performed. The BER plots also show the results for 3 turbo iterations, so it is possible to have a sense of how the turbo iterations improve equalization performance.

Moreover, the transmitted signal was sampled at a frequency of $f_s = 24$ kHz. During the transmission through the UWA channel, the carrier frequency was $f_c = 7.5$ kHz with 5 kHz of bandwidth. To emulate the analog transmission, the transmitted signal is upsampled to $f'_s = \lceil \frac{f_s}{\text{bandwidth}} \rceil f_s = Q f_s = 5 \cdot 24 \text{ kHz} = 120 \text{ kHz}$. Then, the signal is filtered with a pulse-shaping filter, designed as a Parks-McClellan optimal FIR filter, with order 500, passband $[0, 4, 992]$ kHz and stopband $[5, 2392, 12]$ kHz. At the receiver the signal is downsampled by a factor of Q and then processed. These numbers for sampling frequency, carrier frequency, bandwidth, and upsampling rate were based on previous practical experiments described in [57]. Table 5.2 comprises the presented simulation parameters.

Table 5.2: Parameters used on simulations to generate the BER plot.

Simulation Parameters	
Monte Carlo iterations	5000
Bits generated	500
SNR values in dB	$\{0, 2, \dots, 18\}$
Modulation scheme	BPSK
Convolutional code polynomial generator	$g_0(D) = 1 + D^2, g_1(D) = 1 + D + D^2$
Sampling frequency, f_s	24 kHz
Carrier frequency, f_c	7 kHz
Bandwidth	5 kHz
Upsampling rate, Q	5
Length- W $\mathbf{y}[n]$ window	401
Pulse shaping filter	Parks-McClellan optimal FIR, order 500, passband $[0, 4, 992]$ kHz and stopband $[5, 2392, 12]$ kHz.

5.2.1.1 The Effect of Different Values of W in Turbo Equalization

Equation (4.46) from the TEQ section showed that a length- W $\mathbf{y}[n]$ is used for equalization rather than the full-length \mathbf{y} . This is done in order to reduce the computational burden during the multiple iterations of the equalization process. The question that needed to be answered is which value of W to choose to use in the simulations. To answer the question, simulations were performed using different values of W , where $W = W_1 + W_2 + 1$ and for design reasons, $W_1 = W_2$. The result can be seen in Figure 5.5. There were 500 bits generated to be transmitted, and values $W \in \mathcal{W} = \{21, 101, 201, 401, 499\}$ were tested. As the result using $W = 499$ did not represent a significant improvement on the BER, $W = 401$ was chosen to be used in the simulations.

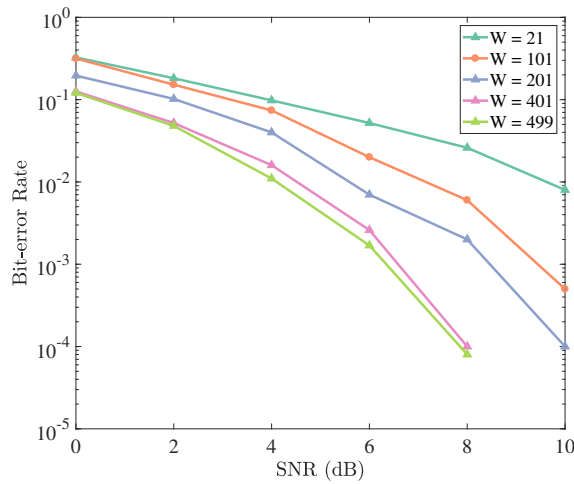
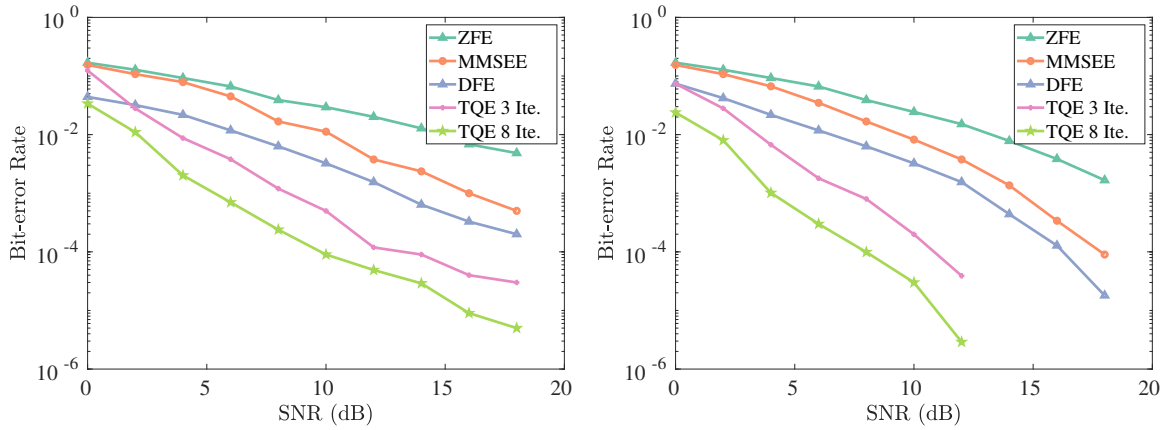


Figure 5.5: BER *versus* SNR plot for different values of W .

5.2.2 Bit-error Rate Plots for the Simulations

The following BER plots show the simulation results made with previously described settings. For each distance at Table 5.1 there is a BER plot where the SNR ranges from 0 dB to 18 dB, with a step of 2 dB. The estimated BER plotted is the average among the 5,000 minimum-phase CIRs used on the Monte Carlo simulations for each distance considered.

Figure 5.6 shows a comparison of two simulations made with the same 1 km scenario. Figure 5.6a presents the result for the simulation using an ensemble of channels containing both minimum-phase and nonminimum-phase CIRs, while Figure 5.6b shows the result for the simulation performed with only minimum-phase CIRs. The last simulation depicts equalizer performances better than the first one. These results may be caused by the fact that the equalizers used are based on second-order statistics (e.g., autocorrelation), which suppress phase information [93], which leads to BER performance degradation when trying to equalize a nonminimum-phase channel. As the purpose of this work is to compare the performance of the equalizers presented in Chapter 4, it was decided to simulate using only minimum-phase channels to see a fair display of their capabilities.



(a) BER for 1 km including nonminimum-phase channels. (b) BER for 1 km minimum-phase channels only.

Figure 5.6: Comparison between two simulations. One containing nonminimum-phase and minimum-phase CIRs, and another simulation using only minimum phase CIRs.

In Figure 5.7a, for the 500 m scenario, the ZFE achieves a BER of 10^{-2} around 11.4 dB of SNR. When compared to ZFE, the MMSEE accomplishes the same BER mark with 8.5 dB of SNR, where this 2.9 dB difference represents a gain of SNR. Analogously, when compared to the ZFE at 10^{-2} of BER, the DFE has a 5.0 dB gain, the 3rd TEQ iteration has a 7.0 dB gain, and the 8th TEQ iteration has a 9.4 dB gain.

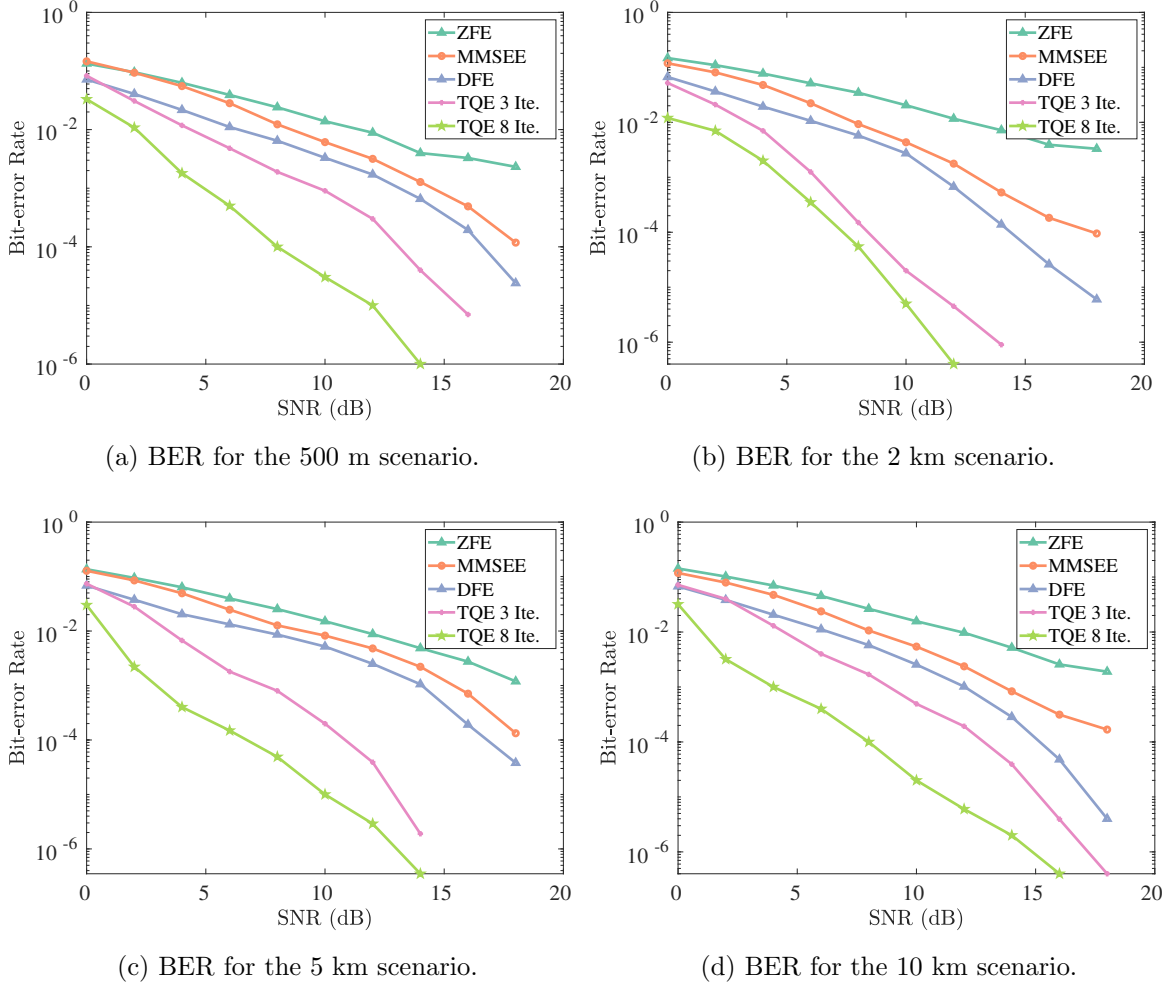


Figure 5.7: Bit-error rate for different distances.

Following the same analysis, the other distances represented in Figures 5.6b and 5.7, the equalizer performances have the same pattern as in the 500 m scenario. Table 5.3 displays the equalizers gain when compared to the SNR necessary to the ZFE achieve 10^{-2} of SNR. It is possible to observe that the results follow the same arrangement, with the 8th and 3rd TEQ outperforming the other equalizers, then come the DFE, MMSEE and ZFE with higher BER for the same SNR values.

Table 5.3: SNR gain (dB) when compared to BER of 10^{-2} for the ZFE.

	Distance (km)				
	0.5	1.0	2.0	5.0	10.0
MMSEE	2.9	3.8	4.8	2.9	3.7
DFE	5.0	6.7	6.5	4.6	5.6
TEQ 3 Ite.	7.0	9.8	9.3	8.5	7.4
TEQ 8 Ite.	9.4	11.6	11.9	11.1	10.8

In a complementary analysis, Table 5.4 assembles the results showing the equalizers' SNR needed to achieve a 10^{-4} BER for all the simulations done. When an equalizer does not accomplish such a BER mark, a hyphen is put in place.

Table 5.4: SNR level (dB) necessary to achieve a BER of 10^{-4} .

	Distance (km)				
	0.5	1.0	2.0	5.0	10.0
ZFE	-	-	-	-	-
MMSEE	18.0	17.8	17.7	18	-
DFE	16.6	16.2	14.3	16.8	15.2
TEQ 3 Ite.	13.1	10.8	8.4	10.8	12.8
TEQ 8 Ite.	7.9	8.0	7.3	6.7	8.1

Chapter 6

Conclusions & Future Work

This work presented in details the UWA channel and its characteristics, the main impairments on transmitting data through the channel and how to model the UWA CIR. Moreover, equalization was proposed as the main technique employed to mitigate the ISI caused by the UWA channel. Finally, simulations were carried out to evaluate the equalizers performances on different UWA channel scenarios.

6.1 Conclusions

There were a few different results presented throughout this work. Figure 4.5 shows how a BPSK constellation behaves after multiple iterations of the TEQ. In Chapter 5, Table 5.1 shows the settings used to generate the channels employed in the simulations, and it is possible to reproduce the CIRs with the same statistical characteristics. Moreover, to justify the use of the parameter W , a simulation is done varying such parameter, and the best suiting one is chosen, comprising BER achievement and computational complexity easement.

For the most anticipated result, the BER *versus* SNR plots for the simulations revealed a pattern, where the TEQ had the best performances, followed by the DFE, MMSEE and the worst one is the ZFE. This pattern is expected because the equalizer computational complexity grows as the BER decreases for each one. The ZFE has the worst performance because it only tries to invert the channel matrix, not even considering the additive noise. On the other hand, the TEQ is

more computationally demanding to account for all iterations.

6.2 Future Work

This work focused on the equalizer performances, evaluating them through simulations. A natural path is to extend what was simulated and develop new scenarios, using richer constellations and exploring more parameters involved in the simulations. It is possible to test different types of FEC; to employ more complex techniques of estimating the CIR, which may result in a more reliable representation of a practical transmission. Another alternative is to explore the equalization on nonminimum-phase channels, using techniques based on higher-order statistics [93], for example.

Moreover, another path for future work is to explore a more practical side. It is possible to apply what was studied here and implement in a real-life functional communication system. It is not an easy path, but surely an interesting one.

Bibliography

- [1] MACCURDY, E., *Notebooks of Leonardo da Vinci*. 1 ed. New York City, George Braziller, 1939.
- [2] NEWTON, I., *Philosophiae Naturalis Principia Mathematica*. 3 ed. London, J. Societatis Regiae ac Typis J. Streater, 1687.
- [3] MEDWIN H., CLAY S. C., *Fundamentals of Acoustical Oceanography*. 1 ed. Cambridge, Academic Press, 1998.
- [4] RAYLEIGH, J., *The Theory of Sound*. 2 ed. Cambridge, Cambridge University Press, 2011.
- [5] URICK, R. J., *Principles of Underwater Sound*. 3 ed. Newport Beach, Peninsula Pub, 1983.
- [6] FROST, G. L., “Inventing Schemes and Strategies: The Making and Selling of the Fessenden Oscillator”, *Technology and Culture*, v. 42, n. 3, pp. 462–488, July 2001.
- [7] MANBACHI, A., COBBOLD, R. S. C., “Development and Application of Piezoelectric Materials for Ultrasound Generation and Detection”, *Ultrasound*, v. 19, n. 4, pp. 187–196, November 2011.
- [8] CURIE, J., CURIE, P., “Development by Pressure of Polar Electricity in Hemihedral Crystals with Inclined Faces”, *Bulletin de la Societe de Minerologique*, v. 3, n. 1, pp. 90, April 1880.
- [9] CURIE, J., CURIE, P., “Contractions and Expansions Produced by Voltages in Hemihedral Crystals with Inclined Faces”, *Comptes Rendus 93*, v. 3, n. 1, pp. 1137–1140, February 1881.

- [10] ZHOU, S., WANG, Z., *OFDM for Underwater Acoustic Communications*. 1 ed. Hoboken, John Wiley & Sons, 2014.
- [11] LICHTÉ, H., “On the Influence of Horizontal Temperature Layers in Seawater on the Range of Underwater Sound Signals”, *Physikalische Zeitschrift*, v. 17, n. 1, pp. 385–389, September 1919.
- [12] LASKY, M., “Review of Undersea Acoustics to 1950”, *The Journal of the Acoustical Society of America*, v. 61, n. 2, pp. 283–297, February 1977.
- [13] KLEIN, E., “Underwater Sound and Naval Acoustical Research and Applications Before 1939.”, *The Journal of the Acoustical Society of America*, v. 43, n. 5, pp. 931–947, July 1968.
- [14] XU, L., XU, T., *Digital Underwater Acoustic Communications*. 1 ed. Massachusetts, Academic Press, 2016.
- [15] BELL, T. G., *Sonar and Submarine Detection*, Technical Report 545, Navy Underwater Sound Laboratory, Newport, 1962.
- [16] QUAZI, A., KONRAD, W., “Underwater Acoustic Communications”, *IEEE Communications Magazine*, v. 20, n. 2, pp. 24–30, March 1982.
- [17] ISTEPANIAN, R. S. H., STOJANOVIC, M., *Underwater Acoustic Digital Signal Processing and Communication Systems*. 1 ed. Berlin, Springer, 2002.
- [18] BAGGEROER, A., MUNK, W., “The Heard Island Feasibility Test”, *Physics Today*, v. 45, n. 9, pp. 22–30, September 1992.
- [19] BRITO, M. P., LEWIS, R. S., BOSE, N., *et al.*, “Adaptive Autonomous Underwater Vehicles: An Assessment of Their Effectiveness for Oceanographic Applications”, *IEEE Transactions on Engineering Management*, v. 1, n. 66, pp. 98–111, February 2019.
- [20] FERRI, G., MUNAFO, A., LEPAGE, K., “An Autonomous Underwater Vehicle Data-driven Control Strategy for Target Tracking”, *IEEE Journal of Oceanic Engineering*, v. 43, n. 2, pp. 323–343, February 2018.

- [21] KAYA, A., YAUCHI, S., “An Acoustic Communication System for Subsea Robot”. In: *Proceedings OCEANS*, pp. 765–770, IEEE, Seattle, September 1989.
- [22] LUO, Y., PU, L., ZUBA, M., *et al.*, “Cognitive Acoustics: Making Underwater Communications Environment-friendly”. In: *Proceedings of the International Conference on Underwater Networks*, pp. 1–2, ACM, Rome, November 2014.
- [23] GUSSEN, C. M. G., DINIZ, P. S. R., CAMPOS, M. L. R., *et al.*, “A Survey of Underwater Wireless Communication Technologies”, *Journal of Communication and Information Systems*, v. 31, n. 1, pp. 242–255, October 2016.
- [24] LURTON, X., *An Introduction to Underwater Acoustics: Principles and Applications*. 2 ed. Berlin, Springer-Verlag Berlin Heidelberg, 2010.
- [25] STOJANOVIC, M., “Underwater Acoustic Communications”. In: *Proceedings of Electro International*, v. 4, pp. 435–440, IEEE, Boston, June 1995.
- [26] LANBO, L., SHENGLI, Z., JUN-HONG, C., “Prospects and Problems of Wireless Communication for Underwater Sensor Networks”, *Wireless Communications and Mobile Computing*, v. 8, n. 8, pp. 977–994, October 2008.
- [27] KATSNELSON, B., PETNIKOV, V., LYNCH, J., *Fundamentals of Shallow Water Acoustics*. 1 ed. New York, Springer-Verlag, 2012.
- [28] BREKHOVSKIKH, L. M., LYSANOV, Y. P., *Fundamentals of Ocean Acoustics*. 3 ed. New York, Springer, 2003.
- [29] LIU C., ZAKHAROV Y. V., C. T., “Doubly Selective Underwater Acoustic Channel Model for a Moving Transmitter/Receiver”, *IEEE Transactions on Vehicular Technology*, v. 61, n. 3, pp. 938–950, March 2012.
- [30] VAN WALREE, P. A., “Propagation and Scattering Effects in Underwater Acoustic Communication Channels”, *IEEE Journal of Oceanic Engineering*, v. 38, n. 4, pp. 614–631, October 2013.
- [31] KILFOYLE, D., BAGGEROER, A., “The State of the Art in Underwater Acoustic Telemetry”, *IEEE Journal of Oceanic Engineering*, v. 25, n. 1, pp. 4–27, January 2000.

- [32] CATIPOVIC, J., “Performance Limitations in Underwater Acoustic Telemetry”, *IEEE Journal of Oceanic Engineering*, v. 15, n. 3, pp. 205–216, July 1990.
- [33] STOJANOVIC, M., “Recent Advances in High-speed Underwater Acoustic Communications”, *IEEE Journal of Oceanic Engineering*, v. 21, n. 2, pp. 125–136, April 1996.
- [34] CHAVES, R. S., MARTINS, W. A., DINIZ, P. S. R., “Modeling and Simulation of Underwater Acoustic Communication Systems”. In: *XXXV Simpósio Brasileiro de Telecomunicações e Processamento de Sinais*, São Pedro, September 2017.
- [35] PROAKIS, J. G., SALEHI, M., *Digital Communications*. 5 ed. New York, McGraw-Hill Education, 2007.
- [36] HAYKIN, S., *Communication Systems*. 4 ed. New York, John Wiley & Sons, Inc., 2001.
- [37] TUCHLER, M., SINGER, A. C., “Turbo Equalization: An Overview”, *IEEE Transactions on Information Theory*, v. 57, n. 2, pp. 920–952, January 2011.
- [38] BELFIORE, C. A., PARK, J. H., “Decision Feedback Equalization”, *Proceedings of the IEEE*, v. 67, n. 8, pp. 1143–1156, August 1979.
- [39] AL-DHAHIR, N., CIOFFI, J., “MMSE Decision-feedback Equalizers: Finite-length Results”, *IEEE Transactions on Information Theory*, v. 41, n. 4, pp. 961–975, July 1995.
- [40] KOETTER, R., SINGER, A. C., TUCHLER, M., “Turbo Equalization”, *IEEE Signal Processing Magazine*, v. 21, n. 1, pp. 67–80, February 2004.
- [41] TUCHLER, M., SINGER, A. C., KOETTER, R., “Minimum Mean Squared Error Equalization Using a Priori Information”, *IEEE Transactions on Signal Processing*, v. 50, n. 3, pp. 673–683, August 2002.
- [42] TUCHLER, M., KOETTER, R., SINGER, A., “Turbo Equalization: Principles and New Results”, *IEEE Transactions on Communications*, v. 50, n. 5, pp. 754–767, August 2002.

- [43] BERROU, C., GLAVIEUX, A., THITIMAJSHIMA, P., “Near Shannon Limit Error-correcting Coding and Decoding: Turbo Codes.” In: *IEEE International Conference on Communications*, pp. 1064–1070, IEEE, Geneva, May 1993.
- [44] ZHENG, Y. R., WU, J., XIAO, C., “Turbo Equalization for Single-carrier Underwater Acoustic Communications”, *IEEE Communications Magazine*, v. 11, n. 53, pp. 79–87, November 2015.
- [45] STOJANOVIC, M., “Underwater Acoustic Communications: Design Considerations on the Physical Layer”. In: *5th Annual Conference on Wireless on Demand Network Systems and Services*, v. 1, pp. 1–10, IEEE, Garmisch-Partenkirchen, January 2008.
- [46] MACKENZIE, K. V., “Nine-term Equation for Sound Speed in the Oceans”, *The Journal of the Acoustical Society of America*, v. 70, n. 3, pp. 807, September 1981.
- [47] DEL GROSSO, V. A., “New Equation for the Speed of Sound in Natural Waters (with Comparisons to other Equations)”, *The Journal of the Acoustical Society of America*, v. 56, n. 4, pp. 1084–1091, August 1974.
- [48] MEDWIN, H., “Speed of Sound in Water : A Simple Equation for Realistic Parameters”, *Journal of the Acoustical Society of America*, v. 58, n. 6, pp. 1975–1977, June 2005.
- [49] THORP, W. H., “Analytic Description of the Low-Frequency Attenuation Coefficient”, *The Journal of the Acoustical Society of America*, v. 42, n. 1, pp. 270, July 1967.
- [50] MELODIA, T., KULHANDJIAN, H., KUO, L.-C., *et al.*, “Advances in Underwater Acoustic Networking”. In: *Mobile Ad Hoc Networking: Cutting Edge Directions, Second Edition*, 2 ed., chapter 11, New York, John Wiley & Sons, pp. 804–854, 2013.
- [51] PREISIG, J., “Acoustic Propagation Considerations for Underwater Acoustic Communications Network Development”, *ACM SIGMOBILE Mobile Computing and Communications Review*, v. 11, n. 4, pp. 2–10, October 2007.

- [52] ANDREA, G., *Wireless Communications*. 1 ed. Cambridge, Cambridge University Press, 2005.
- [53] ARVESON, P. T., VENDITTIS, D. J., “Radiated Noise Characteristics of a Modern Cargo Ship”, *The Journal of the Acoustical Society of America*, v. 107, n. 1, pp. 118–129, January 2000.
- [54] CHITRE, M., POTTER, J., ONG, S.-H., “Optimal and Near-Optimal Signal Detection in Snapping Shrimp Dominated Ambient Noise”, *IEEE Journal of Oceanic Engineering*, v. 31, n. 2, pp. 497–503, April 2006.
- [55] WANG, Z., ZHOU, S., CATIPOVIC, J., *et al.*, “Parameterized Cancellation of Partial-Band Partial-Block-Duration Interference for Underwater Acoustic OFDM”, *IEEE Transactions on Signal Processing*, v. 60, n. 4, pp. 1782–1795, April 2012.
- [56] STOJANOVIC, M., “On the Relationship Between Capacity and Distance in an Underwater Acoustic Communication Channel”. In: *1st ACM international Workshop on Underwater Networks*, v. 1, pp. 41–47, ACM, Los Angeles, October 2006.
- [57] PINHO, V. M., CHAVES, R. S., CAMPOS, M. L. R., “On Equalization Performance in Underwater Acoustic Communication”. In: *XXXVI Simpósio Brasileiro de Telecomunicações e Processamento de Sinais*, SBrT, Campina Grande, July 2018.
- [58] LATHI, B. P., *Modern Digital and Analog Communication Systems*. 2 ed. New York, Oxford University Press, Inc., 1995.
- [59] COSTELLO, D. J., FORNEY, G. D., “Channel Coding: The Road to Channel Capacity”, *Proceedings of the IEEE*, v. 95, n. 6, pp. 1150–1177, June 2007.
- [60] SHANNON, C. E., “A Mathematical Theory of Communication”, *Bell System Technical Journal*, v. 27, n. 3, pp. 379–423, July 1948.
- [61] WICKER, S., *Error Control Systems for Digital Communication and Storage*. 1 ed. Upper Saddle River, Prentice Hall, 1995.

- [62] LIN, S., COSTELLO, J., *Error Control Coding*. 1 ed. Upper Saddle River, Prentice Hall, 1983.
- [63] ROTH, R., *Introduction to Coding Theory*. 1 ed. Cambridge, Cambridge University Press, 2006.
- [64] GALLAGER, R., *Principles of Digital Communication*. 1 ed. Cambridge, Cambridge University Press, 2008.
- [65] ANDREWS, K., HEEGARD, C., KOZEN, D., *A Theory of Interleavers*, Technical Report 4, Cornell University, Ithaca, 1997.
- [66] CHAVES, S., MARTINS, W. A., DINIZ, R., *Modelagem e Simulação de Sistemas de Comunicação Acústica Subaquáticos*. Undergraduate thesis, Federal University of Rio de Janeiro, Rio de Janeiro, 2016.
- [67] CHITRE, M., “A High-frequency Warm Shallow Water Acoustic Communications Channel Model and Measurements”, *The Journal of the Acoustical Society of America*, v. 122, n. 5, pp. 2580–2586, November 2007.
- [68] RADOSEVIC, A., PROAKIS, J. G., STOJANOVIC, M., “Statistical Characterization and Capacity of Shallow Water Acoustic Channels”. In: *OCEANS 2009 Europe*, pp. 1–8, IEEE, Bremen, May 2009.
- [69] BAHRAMI, N., KHAMIS, N. H. H., BAHAROM, A. B., “Study of Underwater Channel Estimation Based on Different Node Placement in Shallow Water”, *IEEE Sensors Journal*, v. 16, n. 4, pp. 1095–1102, February 2016.
- [70] TOMASI, B., CASARI, P., BADIA, L., *et al.*, “A Study of Incremental Redundancy Hybrid ARQ over Markov Channel Models Derived from Experimental Data”. In: *5th ACM International Workshop on Underwater Networks*, pp. 1–8, ACM Press, New York, September 2010.
- [71] YANG, W.-B., YANG, T. C., “High-frequency Channel Characterization for M-ary Frequency-shift-keying Underwater Acoustic Communications”, *The Journal of the Acoustical Society of America*, v. 120, n. 5, pp. 2615–2621, November 2006.

- [72] KULHANDJIAN, H., MELODIA, T., “Modeling Underwater Acoustic Channels in Short-range Shallow Water Environments”. In: *Proceedings of the International Conference on Underwater Networks Systems*, pp. 1–5, ACM Press, New York, November 2014.
- [73] OHNO, S., “Performance of Zero-forcing Equalizers for Single-carrier Zero-padded Transmissions over Multipath Fading Channels”. In: *IEEE International Conference on Acoustics, Speech, and Signal Processing*, pp. iv–1017, IEEE, Montreal, May 2004.
- [74] VIRK, S. S., NATHAN, P., “Comparative Performance Analysis of Zero Forcing, Minimum Mean Square Error and Decision Feedback Equalizer”. In: *International Conference on Green Computing, Communication and Conservation of Energy*, pp. 136–139, IEEE, Chennai, December 2013.
- [75] KAY, S. M., *Fundamentals of Statistical Signal Processing: Estimation Theory*. 1 ed. Upper Saddle River, Prentice-Hall, 1993.
- [76] DINIZ, P. S. R., MARTINS, W. A., LIMA, M. V. S., *Block Transceivers: OFDM and Beyond*, Synthesis Lectures on Communications. 1 ed. Colorado Springs, Morgan & Claypool Publishers, 2012.
- [77] AUSTIN, M. E., *Decision-feedback Equalization for Digital Communication over Dispersive Channels.*, Technical Report 437, Research Laboratory of Electronics, Massachusetts Institute of Technology, Cambridge, 1967.
- [78] GOLUB, G. H., LOAN, C. F. V., *Matrix Computations*. 3 ed. Baltimore, Johns Hopkins University Press, 1996.
- [79] TREFETHEN, L. N., BAU, D., *Numerical Linear Algebra*. 1 ed. Philadelphia, SIAM, 1997.
- [80] VOOIS, P., LEE, I., CIOFFI, J., “The Effect of Decision Delay in Finite-length Decision Feedback Equalization”, *IEEE Transactions on Information Theory*, v. 42, n. 2, pp. 618–621, March 1996.

- [81] DOUILLARD, C., JÉZÉQUEL, M., BERROU, C., *et al.*, “Iterative Correction of Intersymbol Interference: Turbo-equalization”, *European Transactions on Telecommunications*, v. 6, n. 5, pp. 507–511, September 1995.
- [82] BENEDETTO, S., DIVSALAR, D., MONTORSI, G., *et al.*, “Serial Concatenated Trellis Coded Modulation with Iterative Decoding”. In: *International Symposium on Information Theory*, pp. 8–16, IEEE, Ulm, June 1997.
- [83] BENEDETTO, S., MONTORSI, G., “Unveiling Turbo Codes: Some Results on Parallel Concatenated Coding Schemes”, *IEEE Transactions on Information Theory*, v. 42, n. 2, pp. 409–428, March 1996.
- [84] XIAODONG, W., POOR, H., “Iterative (Turbo) Soft Interference Cancellation and Decoding for Coded CDMA”, *IEEE Transactions on Communications*, v. 47, n. 7, pp. 1046–1061, July 1999.
- [85] XU, F., KHALIGHI, M.-A., BOURENNANE, S., “Coded PPM and Multipulse PPM and Iterative Detection for Free-space Optical Links”, *Journal of Optical Communications and Networking*, v. 1, n. 5, pp. 404, October 2009.
- [86] SING, A., NELSON, J., KOZAT, S., “Signal Processing for Underwater Acoustic Communications”, *IEEE Communications Magazine*, v. 47, n. 1, pp. 90–96, January 2009.
- [87] SIFFERLEN, J., SONG, H., HODGKISS, W., *et al.*, “An Iterative Equalization and Decoding Approach for Underwater Acoustic Communication”, *IEEE Journal of Oceanic Engineering*, v. 33, n. 2, pp. 182–197, April 2008.
- [88] WON CHOI, J., DROST, R. J., SINGER, A. C., *et al.*, “Iterative Multi-channel Equalization and Decoding for High Frequency Underwater Acoustic Communications”. In: *5th IEEE Sensor Array and Multichannel Signal Processing Workshop*, pp. 127–130, IEEE, Darmstadt, July 2008.
- [89] OTNES, R., EGGEN, T., “Underwater Acoustic Communications: Long-term Test of Turbo Equalization in Shallow Water”, *IEEE Journal of Oceanic Engineering*, v. 33, n. 3, pp. 321–334, July 2008.

- [90] BAHL, L. R., COCKE, J., JELINEK, F., *et al.*, “Optimal Decoding of Linear Codes for Minimizing Symbol Error Rate”, *IEEE Transactions on Information Theory*, v. 20, n. 2, pp. 284–287, March 1974.
- [91] FORNEY, G., “Maximum-likelihood Sequence Estimation of Digital Sequences in the Presence of Intersymbol Interference”, *IEEE Transactions on Information Theory*, v. 18, n. 3, pp. 363–378, May 1972.
- [92] EY, E., *SiPLAB Internal Report*, Technical Report 1, Universidade do Algarve, Faro, 2012.
- [93] BLOM, K. C. H., GERARDS, M. E. T., KOKKELER, A. B. J., *et al.*, “Nonminimum-phase Channel Equalization Using All-pass CMA”. In: *24th Annual International Symposium on Personal, Indoor, and Mobile Radio Communications*, pp. 1467–1471, IEEE, London, September 2013.